Applied Physics A (2025) 131:859
https://doi.org/10.1007/s00339-025-08975-0

Applied Physics A
Materials Science & Processing

Review of progress in inorganic electron transport layers for perovskite solar cell applications

Abubakar Sadiq Yusuf[1,2,3] · **Martin Markwitz**[2,4,5] · **Zhan Chen**[1] · **Maziar Ramezani**[1] · **John V. Kennedy**[2,5] · **Holger Fiedler**[2]

Received: 8 July 2025 / Accepted: 17 September 2025

Abstract

Perovskite solar cells (PSCs) have emerged as a revolutionary photovoltaic technology, achieving remarkable power conversion efficiencies (PCEs) above 26.61%, while offering low-cost and scalable fabrication. Among the critical components of PSCs, the electron transport layer (ETL) plays a vital role in charge extraction, transport, and recombination suppression. This review provides a comprehensive analysis of recent advancements in inorganic ETLs, particularly focusing on widely studied materials such as TiO_2, SnO_2, and ZnO. While TiO_2 has historically been the benchmark ETL, challenges such as high-temperature processing and photocatalytic instability have led researchers to explore alternative materials. SnO_2 has gained prominence due to its superior electron mobility, low temperature processability, and excellent optical transparency, making it a strong candidate for high-performance PSCs. ZnO, with its high conductivity and facile synthesis, also shows promise, but faces stability concerns. The review further highlights the significance of surface modifications, doping strategies, and interface engineering to optimize charge transport dynamics and enhance device longevity. Additionally, we discuss emerging alternatives and future perspectives on scalable, cost-effective, and stable ETLs that could drive PSCs toward commercialization. By bridging fundamental material properties with device performance, this work provides insights into the next generation of high-efficiency and durable PSCs.

Keywords Electron transport layers · SnO_2 · TiO_2 · ZnO · Doping · Surface modification · Perovskite solar cells

1 Introduction

The scarcity of conventional energy sources and the escalating environmental issues pose significant hurdles to sustainable human progress [1]. Solar energy, as a novel kind of renewable energy, offers vast developmental potential [2]. Due to the remarkable optoelectronic properties of perovskites, PSCs are regarded as revolutionary next-generation solar cell technology [3–5]. With an exceptional increase in PCE from 3.8% [6] to 26.61% [7] over the previous 10 years, as well as notable improvements in operational stability, perovskite material and device stacks have shown tremendous potential for commercial applications [3, 8, 9]. Since PSCs were first produced from dye-sensitized solar cells by employing perovskite absorbers instead of dye sensitizers, the n-i-p configuration is thought to be the typical device structure among the numerous PSC device topologies [3, 6, 10, 11]. The transparent conductive oxide (TCO), dense and/or mesoporous n-type ETL, the perovskite absorber layer, p-type hole transport layer (HTL), back

✉ Abubakar Sadiq Yusuf
Abubakar.yusuf@autuni.ac.nz

1 School of Engineering, Computer and Mathematical Sciences, Auckland University of Technology, PO Box 92006, Auckland 1142, New Zealand

2 National Isotope Centre, GNS Science, PO Box 30368, Lower Hutt 5010, New Zealand

3 School of Physical Sciences, Department of Physics, Federal University of Technology, PMB 65, Minna, Niger State, Nigeria

4 School of Chemical and Physical Sciences, Victoria University of Wellington, PO Box 600, Wellington 6140, New Zealand

5 The MacDiarmid Institute for Advanced Materials and Nanotechnology, Victoria University of Wellington, PO Box 600, Wellington 6140, New Zealand

Published online: 14 October 2025

contact electrode, and occasionally additional interfacial layers to improve performance are the main components of an n-i-p device stack. An efficient ETL/HTL can reduce interfacial charge buildup and recombination. The charge transport layers encompassing ETL and HTL are crucial for sorting and extracting specific photogenerated carriers and inhibiting countercharge carriers [12]. The perovskite layer is coated on the n-type ETL in an n-i-p-structured PSC, and the ETLs surface area and surface chemistry directly impact the deposition and quality of the perovskite layer.

Organic electron transport materials include polymers, fullerene derivatives, and norfullerene small molecules suitable for low-temperature manufacturing and flexible perovskite solar cells. The characteristics of organic materials are greatly influenced by their structures, which subsequently dictate the efficacy of devices. In planar perovskite solar cells, organic ETLs, particularly fullerene and its derivatives, are predominantly used, with PCBM being the most frequently employed ETL. The first use of PCBM as an ETL in PSCs was documented by Jeng et al. this work effectively illustrated the use of PCBM as an ETL in the construction of NiO_x/$MAPbI_3$/PCBM perovskite solar cells, achieving a PCE of 7.8% [13]. N-type organic small molecules as ETLs have garnered significant interest among organic materials due to the simplicity of their synthesis and the ability to modify their energy level bands to align with the energy levels of the light-absorbing perovskite layer. Moreover, including sulfur species into their structure by establishing S-I or (S-Pb) bonds may enhance the interfacial contact between the ETL and perovskite [14]. Lee et al. created self-assembled organic nanocomposites (SAONs) as a novel ETL using n-type polyelectrolytes and fullerene derivatives. This method effectively produced optimal and self-organizing ETLs that operate both as electron acceptors and surface work function modifiers [15]. A PCE of 17.3% was achieved in PSCs using printed silver ammonium oxide nanofilms. Notwithstanding the benefits of organic ETLs like PCBM and SAONs in planar PSCs, identifying appropriate ETL candidates that can be synthesized economically and processed quickly to provide high-performance products remains a significant challenge [15]. Organic n-type materials serve as ETLs and provide benefits like excellent flexibility and straightforward solution processing. Nonetheless, these materials exhibit some disadvantages, such as inadequate thermal, optical, and moisture stability, as well as elevated costs [16].

Inorganic electron-transport materials are regarded as substitutes for ETLs in PSCs. Their superior stability, lower cost, wide bandgap, deeper conduction band, and high electron mobility make them optimal candidates for use as ETLs in PSCs. At present, the majority of highly efficient PSCs and certified devices employ the conventional n–i–p configuration, common inorganic ETMs include TiO_2 [17, 18], ZnO [19] and SnO_2 [20]. Previous reviews have not sufficiently emphasized the critical role of interface engineering in minimizing defects and reducing recombination rates at the ETL surface. This aspect is essential for maximizing ETL efficiency in PSCs and achieving high-performance device operation. While TiO_2, ZnO and SnO_2 remain the most widely studied ETLs, their inherent limitations such as the need for high-temperature annealing highlight the need for alternative materials and fabrication techniques. However, these alternatives have not received adequate attention in prior studies, leaving a gap in the exploration of more efficient and scalable solutions. Additionally, the chemical stability and hydrophobicity of ETLs, crucial for preventing moisture infiltration and unwanted reactions with perovskite materials, have often been overlooked. Ensuring these properties is fundamental to improving the long-term durability and operational stability of PSCs. Another critical yet underexplored factor is the impact of crystal orientation on charge carrier mobility within SnO_2 films [21]. The choice of precursor type and crystal structure significantly influences ETL performance, and a deeper understanding of these relationships can lead to more effective optimization strategies.

Leveraging on these material level considerations, recent advances in photovoltaic materials and architectures are pushing device performance and deployment into new directions, with perovskite-based technologies particularly all-perovskite and perovskite/silicon tandems continue to lead efficiency gains while industry efforts focus on scaling, encapsulation and long-term stability for real-world use [22, 23]. At the same time, lead-free and tin-based perovskites, and flexible/ultra-thin perovskite modules, are receiving heightened attention as routes to reduce toxicity and enable new form factors (indoor harvesting, building-integrated and wearable photovoltaics) [24]. Complementary trends include record-breaking large-area cells and industry investments aimed at commercialization, underscoring the shift from lab-scale champions to manufacturable products. In parallel, the field of solar-driven water photo decontamination has matured from proof-of-concept photocatalysts to hybrid, reactor-level solutions that combine adsorption, membrane filtration, interfacial solar evaporation and engineered photocatalyst support heterojunctions to improve charge separation, broaden light absorption, and enable scalable pollutant removal under natural sunlight [25, 26].

In this work, we have comprehensively reviewed and demonstrated the superiority of SnO_2 as an ETL in PSCs by systematically comparing key ETLs such as TiO_2 and ZnO. Our analysis highlights SnO_2 exceptional electron mobility, which significantly enhances charge transport compared to conventional ETLs. We emphasize the critical role of

interface engineering in minimizing defects and improving charge extraction, addressing a key gap in previous studies. Furthermore, we explore advancements in surface modification techniques that effectively reduce interfacial recombination, leading to improved stability and efficiency of SnO_2-based ETLs. By presenting these insights, this review reinforces SnO_2 position as a leading ETL for high-performance PSCs and provides a valuable foundation for future research aimed at further optimizing device performance.

2 Overview of inorganic ETLs development for perovskite solar sells

The energy bandgap, electron affinity, doping densities of electrons and holes, and the thickness of the ETL delineate the essential attributes of an ETL for optimal photovoltaic performance. The performance optimization of PSCs is contingent upon these constraints. In addition to being mass-producible and cost-effective, the ETL material must exhibit high electron mobility, substantial optical transparency, and appropriate energy-level alignment for efficient electron transport and hole blocking. The most often studied ETLs, such as phenyl-C61-butyric acid methyl ester (PCBM) and C60, have mostly included n-type semiconducting oxides including TiO_2, SnO_2, ZnO, and In_2O_3, as well as organic materials [6, 10, 27–29]. The appropriate band energy alignment with the perovskite layer, high transmittance with a broad bandgap, and high conductivity are some of the essential characteristics of ETLs. Due to its proven deposition techniques and excellent optoelectronic characteristics, the compact TiO_2/mesoporous TiO_2 stack has historically been a crucial part of effective n-i-p PSCs. However, TiO_2 and SnO_2 have limitations that might prevent PSCs from being commercialized, such as photocatalytic characteristics under light and the need for high temperature annealing to produce adequate crystallinity [30]. Numerous studies have looked at potential replacements for TiO_2, focusing on low-cost, easily repeatable, and chemically stable production procedures that are simple and low temperature.

With the best PCE of SnO_2-based n-i-p PSCs above 26.61% [31], TiO_2, ZnO, and SnO_2 are acknowledged as potential ETLs with increasing attention recently; TiO_2 and SnO_2 ETLs are outstanding candidates for highly efficient and stable PSCs due to their advantageous properties, including a wide bandgap with high transmittance, excellent charge mobility, suitable band offsets in relation to conventional perovskites, low-temperature processable synthesis, and suitable chemical stability [32, 33]. Figure 1 shows the evolution of using TiO_2 and SnO_2 in perovskite solar cells. Various ETLs, such as TiO_2 [34], ZnO_2 [35], and SnO_2 [36], are used as ETL materials. Among these, TiO_2 is commonly used due to its simple device structure, high thermal stability, low cost, and high compatibility with flexible substrates [37, 38]. However, insufficient charge separation at the interface between the perovskite layer has been one of the main issues with TiO_2 besides the low electron mobility and high surface defect density [39, 40]. In this review, we have omitted alternative ETLs based on criteria such as reduced effectiveness, reliability, compatibility with specific substrates like FTO, or insufficient performance in terms of charge extraction, shunt resistances, recombination currents, or wetting behavior on various surfaces. Hence, the primary objective of the review is to emphasize the most favorable ETLs for enhancing the efficiency of perovskite solar cells, while discarding those that fail to satisfy the acceptable standards or demonstrate poorer qualities [41].

Consequently, ETL development has emerged as a significant priority for producing highly reliable and efficient n-i-p PSCs. Effective CBM adhesion to lead halide perovskite has been accomplished by SnO_2, hence enabling a minor open-circuit voltage to be negative. Furthermore, femtosecond transient absorption and UV spectroscopy measurements indicate that SnO_2 exhibits superior electron extraction compared to TiO_2. Due to the substantial band gap of about 3.5 eV compared to 3.0 eV of TiO_2, SnO_2 mostly permits the passage of visible light. The exceptional UV light protection of SnO_2 arises from its ability to inhibit UV light absorption. SnO_2 has a two-order-of-magnitude superior bulk electron mobility compared to TiO_2 [18]. SnO_2 low-temperature manufacturing is straightforward and suitable for extensive commercialization [42]. Table 1 delineates the advantages and disadvantages of frequently used ETLs in PSCs for enhanced comprehension.

Table 1 serves as a critical reference for comparing the electrical properties of different inorganic ETLs, including TiO_2, ZnO, and SnO_2. By analyzing the data presented in this table, researchers and scientists can gain a deeper understanding of how various ETLs influence the performance of PSCs. The key parameters to focus on include electron mobility, CBM, bandgap energy, and processing temperature, as they directly impact charge transport, recombination losses, and device stability [45]. Each parameter plays a distinct role in optimizing ETL performance, and evaluating their values helps in selecting the most suitable ETL for achieving high efficiency and long-term stability in PSCs. Among these parameters, electron mobility is one of the most critical because it determines how efficiently electrons can be transported through the ETL. A higher electron mobility ensures faster charge extraction and reduces recombination losses, leading to improved PCE. Typically, ETLs with electron mobility values in the range of 10^{-2} to 10^{2} $cm^2|V^{-1}|$ s^{-1} are considered suitable for high-performance PSCs. SnO_2, for example, exhibits significantly

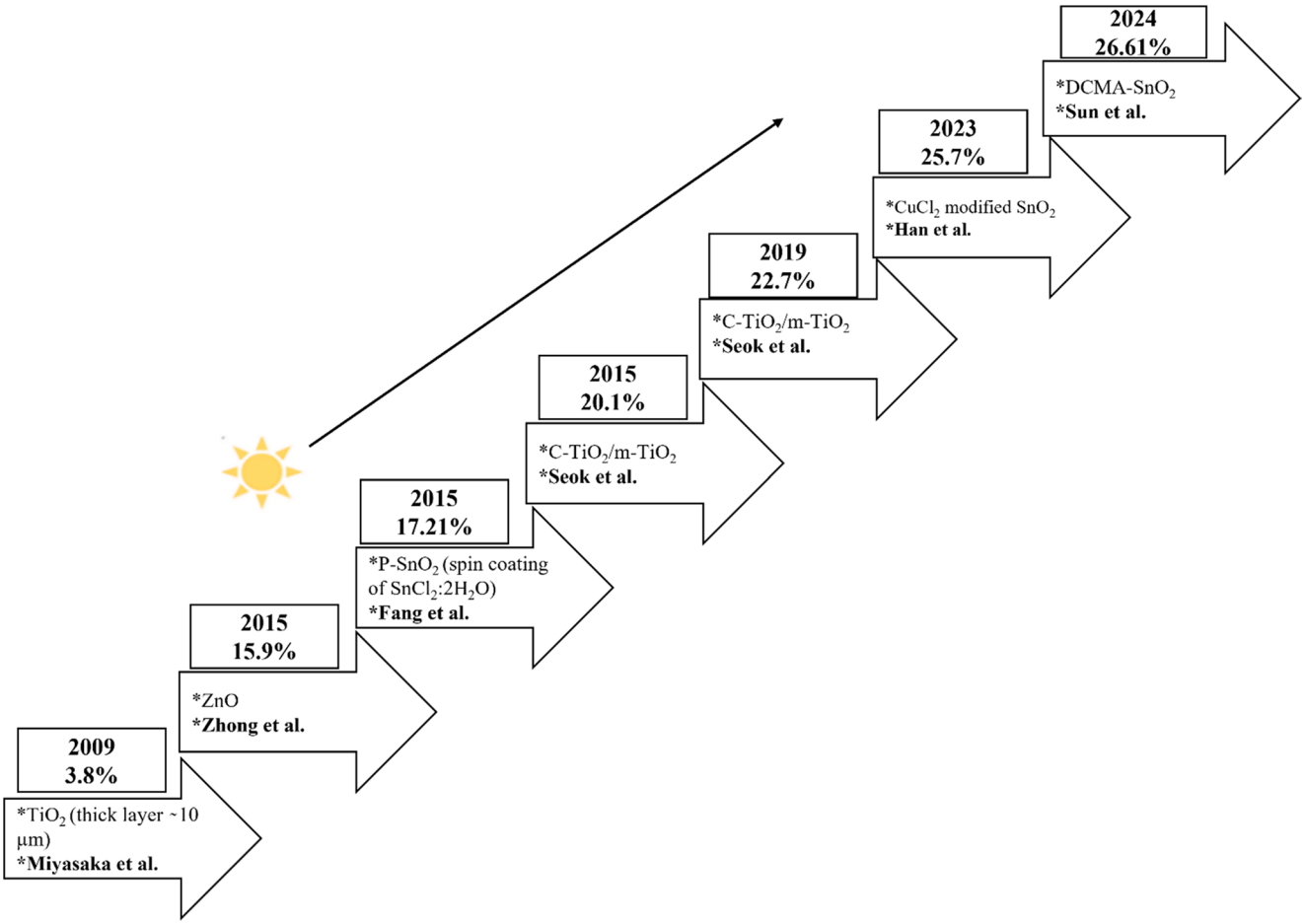

Fig. 1 Recent developments in PSCs incorporating TiO_2, ZnO, and SnO_2 as ETLs

Table 1 Comparison between the electrical properties of TiO_2, ZnO, and SnO_2 [43, 44]

	TiO_2	ZnO	SnO_2
Crystal structure	Rutile, anatase, brookite	Rocksalt, zinc blende, wutzite	Rutile
Energy band gap (eV)	3.0–3.2	3.2–3.3	3.50–4.0
Surface work function (eV)	4.5–5.0	4.45–5.30	4.71–5.33
Electron mobility ($cm^2\ V\ s^{-1}$)	0.1–4.0	Bulk ZnO: 205–300; Nanowire: 1000	240
Refractive index	2.5	2.0	2.0
Electron effective mass (m*)	9	0.26	0.3
Relative dielectric constant	170	8.5	9.6
Electron diffusion coefficient ($cm^2\ s^{-1}$)	Bulk TiO_2: 0.5; nanoparticle: 10^{-8}–10^{-4}	Bulk ZnO: 5.2; nanoparticle film: 1.7×10^{-4}	nanoparticle film: 6.22×10^{-6}

higher electron mobility up to 240 $cm^2|V^{-1}|s^{-1}$ compared to TiO_2 (~ 1 $cm^2|V^{-1}|\ s^{-1}$), making it a superior choice for ETL applications [46]. Another crucial parameter is the CBM, which should be well-aligned with the perovskite layer to facilitate efficient electron transfer while blocking hole recombination. A CBM range of −4.0 to −4.5 eV is ideal to ensure effective charge extraction without energy mismatches that could hinder performance. SnO_2, with a CBM of approximately − 4.2 eV, provides excellent band alignment with common perovskite materials, making it an optimal candidate for ETLs. Additionally, bandgap energy is an important consideration because it affects optical transparency and electron selectivity. A wide bandgap greater than 3.2 eV is preferred to minimize parasitic absorption and ensure that the maximum amount of light reaches the perovskite absorber layer. TiO_2, ZnO, and SnO_2 all have suitable bandgaps, typically in the range of 3.0 to 3.8 eV, making them effective ETLs in PSCs [47, 48].

It is highly recommended to emphasize the significance of simulation-based studies in advancing perovskite solar cell research, particularly when exploring the use of inorganic ETLs. These simulations play a crucial role in understanding device behavior, optimizing material combinations, and guiding experimental efforts toward more efficient and stable solar cell designs. Recent simulation-based investigations have confirmed the critical role of inorganic ETLs in boosting perovskite solar cell performance. For example, SCAPS-1D studies reveal that SnO_2 ETLs, especially at optimized ultrathin thicknesses (~ 10 nm), deliver outstanding simulated performance $V_{OC} \approx 1.118$ V, $J_{SC} \approx 26.95$ mA/cm^2, FF ≈ 78.1%, and PCE ≈ 23.5% [49]. Meanwhile, ZnO ETLs in lead-free perovskite systems achieve J_{SC} ≈ 27 mA/cm^2, exceptional FF (~ 88%), and PCE up to ~ 24.8%. In contrast, TiO_2 ETLs, while common, suffer from optical losses; their optimal simulated cells reach $V_{OC} \approx$ 1.06 V, $J_{SC} \approx 10.7$ mA/cm², FF ≈ 80.9%, and PCE ≈ 9.2%. Additionally, simulations demonstrate that engineering ETL interfaces such as using ZnO/AZO bilayers can significantly elevate performance metrics (e.g., V_{OC} to ~ 1.09 V, J_{SC} to ~ 20.6 mA/cm^2, FF ~ 72%, PCE ~ 16.1%). Moreover, facet-engineered SnO_2 layers in SCAPS models have simulated PCEs of ~ 20.3% with improved charge extraction and device stability [50].

Reza et al. study reveals that the ZnO ETL was optimized by analyzing key photovoltaic parameters, helping to narrow down the most promising device structure. Once the best performing ETL was established, each of the three HTLs was tested to see which combination yielded the highest efficiency. Several factors were varied during this process, including the thickness of the absorber and ETL layers, the defect density in the absorber, and the doping levels in both the ETL and HTL. From this analysis, the device structure using Sb_2S_3 as the HTL with the full stack being Al/FTO/ZnO/Ca_3AsI_3/Sb_2S_3/Ni emerged as the top performer, reaching PCE of around 29.12%, which was higher than the other two configurations. After identifying the best-performing device, the study further examined how factors such as temperature, charge carrier generation and recombination, and resistive losses series and shunt resistance influenced the performance. The comparison of *J-V* curves and QE spectra between the original and improved designs clearly showed that the ZnO-based ETL significantly contributed to higher efficiency [51]. Rahim et al. evaluated and optimize the performance of the device by incorporating SnO_2 as the ETL structure consisting of ITO/SnO_2/$CH_3NH_3PbI_3$/CuSCN; it was determined that the device achieved optimal performance under the following conditions: a working temperature of 300 K, a SnO_2 layer thickness of 100 nm, a donor doping concentration of 10^{17} cm^{-3} in the ETL, an acceptor doping concentration of 10^{18} cm^{-3} in the HTL, and a low defect density of 10^{14} cm^{-2} at the ETL/absorber interface. Under these optimized parameters, the simulated PCE reached an impressive 24.14% [52]. Basit et al. demonstrated, in their recent simulation results, an optimized performance with a PCE of 21.93%, FF of 77.50%, a J_{SC} of 34.05 mA/cm^2, and a V_{OC} of 0.83 V. These promising outcomes highlight the potential of tin-based perovskite solar cells as a viable alternative to their lead-based counterparts. The findings offer valuable insights for future research focused on improving device efficiency, enhancing long-term stability, and narrowing the performance gap between lead-free and conventional PSCs [53]. Meskini et al. results showed that introducing a small amount of Ti_3C_2 MXene (1.0 wt‰) into the SnO_2 ETL significantly improved device performance. In particular, the cell structure ITO/ETL/$CH_3NH_3PbI_3$/Spiro-OMeTAD/Ag, with the modified SnO_2_Ti_3C_2 ETL, achieved an impressive PCE of 27.81% [54].

These findings highlight that simulation-based studies offer high granularity and, in some cases, predictive power that guide experimentalists toward the most promising inorganic ETL materials and architectures. By integrating such virtual insights into material selection, thickness optimization, and interface engineering, your work can both align with state-of-the-art trends and convincingly argue for the role of simulations in accelerating PSC innovation.

2.1 Electron transport layer charge conduction in perovskite solar cell

Apart from being a light-absorbing material inside the device, the perovskite light absorption layer has bipolar charge transport characteristics and acts as both an electron and hole transport medium. In a standard perovskite solar cell, sunlight absorption excites electrons from the valence band to the conduction band, generating excitons and holes. At the perovskite/ETL interface, these excitons then separate to produce free charges. Under the effect of the intrinsic electric field, electrons are moved from the conduction band of the perovskite layer to the conduction band of the ETL being gathered by the ITO electrode. Minimizing charge recombination is a key strategy for improving device performance as free charges often recombining at the interface and within the internal defects during transport [55], usually consisting of an n-type inorganic semiconductor material, the ETL in conventional PSCs. With electrons undergoing directed diffusion and drift movement owing to the impact of concentration gradients and built-in electric fields, inorganic electron transport materials generally show better electron mobility than organic electron transport materials (Fig. 2(**a**) [56].

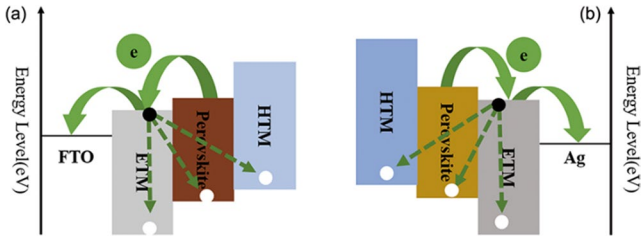

Fig. 2 Illustrates the schematic representation of the electron transport process in (**a**) regular and (**b**) inverted perovskite solar cells

2.2 Charge dynamics within the electron transport layer of perovskite solar cells

The perovskite captures light and produces excitons, which are then dissociated at the interface between the perovskite and the ETL. This process involves the transfer of electrons from the conduction band of the perovskite layer to the LUMO level of the electron transport material, ultimately leading to their collection by the metal electrode in the trans-PSC. Generally regarded as an n-type organic semiconductor, the electron transport material utilized in the trans-PSC. The electron mobility in n-type organic semiconductors is generally limited due to the necessity for electrons to overcome a considerable potential barrier, with their transmission predominantly dependent on the conjugated orbitals that exist between organic molecules (Fig. 2(**b**) [57].

2.3 Function and impact of the electron transport layer in perovskite solar cells

In PSCs, ETL is essential for the extraction and transport of photogenerated electrons, while simultaneously obstructing holes and mitigating charge recombination. The efficacy of electron extraction and collection, hysteresis in current-voltage measurements, and overall device stability are intricately connected to the characteristics of the ETL. In comparison to TiO_2, SnO_2 has surfaced as a viable alternative ETL owing to its enhanced stability, elevated electron mobility, and improved energy level alignment with perovskite materials [58]. In contrast to TiO_2, which experiences oxygen vacancies (Ti^{3+} defect states) that lead to instability during UV exposure, SnO_2 demonstrates a reduced density of deep trap states, hence decreasing non-radiative recombination and improving device durability. TiO_2-based PSCs deteriorate swiftly under UV irradiation owing to the creation of oxygen vacancies and interactions within charge transfer complexes (O_2–Ti^{4+}), resulting in diminished performance. Conversely, SnO exhibits less vulnerability to degradation processes, making it a more durable ETL option for prolonged operation [59].

Under UV radiation, TiO_2 has a bifurcated degradation process attributed to defect-assisted charge trapping and perovskite disintegration. SnO_2 exhibits enhanced robustness owing to its reduced density of oxygen vacancies, which alleviates deep trap formation and charge buildup at the interface. Moreover, the wide bandgap of SnO_2 (about 3.6–4.0.6.0 eV) guarantees little parasitic absorption, hence enhancing light consumption in PSCs. In typical PSCs, a SnO_2 ETL with an optimized shape enhances perovskite crystallization quality, hence reducing interfacial recombination. In inverted PSCs, a thick, pinhole-free SnO_2 ETL offers superior coverage for the perovskite layer while guaranteeing good ohmic contact with the upper electrode. Furthermore, contaminants and flaws inside the SnO_2 layer might affect the efficiency of photoelectric conversion. Donor and acceptor impurities may enhance charge carrier density and conductivity, whereas defects may create recombination sites that reduce carrier lifespan [60].

3 New material for the electron transfer layer in perovskite solar cells

3.1 Advancements in TiO2, SnO2, and ZnO electron transport layers

TiO_2, SnO_2, and ZnO are pivotal ETL materials in optoelectronic devices like PSCs, organic solar cells, and LEDs, valued for their high electron mobility, suitable band alignment, and stability. Recent advancements in experimental and simulation-based studies have significantly enhanced their performance, stability, and scalability. This report explores these developments, focusing on experimental findings, simulation insights, and comparative analyses of TiO_2, SnO_2, and ZnO ETLs. Experimental and simulation studies have highlighted critical advancements in SnO_2 and ZnO, as well as hybrid and doped formulations, to overcome intrinsic limitations of each material. The development of these ETLs is increasingly driven by both experimental thin-film engineering and numerical simulation platforms (e.g., SCAPS-1D, wxAMPS, or TCAD tools) that predict behavior under realistic device operating conditions [61, 62].

TiO_2 has historically been used due to its suitable conduction band level (~−4.0 eV), chemical stability, and low cost. However, its relatively low electron mobility (~ 0.1–4.1 $cm^2|V^{-1}|\ s^{-1}$) and tendency to catalyze photocatalytic degradation under UV exposure have limited its further application in high-efficiency PSCs. Experimental advancements now focus on modifying the morphology and crystallinity of TiO_2 via low-temperature synthesis, enabling compatibility with flexible substrates. Doping with Nb, F, or Ta has been shown to enhance its conductivity and suppress charge recombination. In parallel, heterostructures

like TiO_2/SnO_2 bilayers are being developed to leverage the high surface area of mesoporous TiO_2 with the smoother interface of SnO_2 [63–65]. From a simulation perspective, studies now integrate the effect of defect states, trap-assisted recombination, and interface energetics to model how oxygen vacancies or surface hydroxylation affect performance. Simulations further validate the role of compact vs. mesoporous TiO_2 layers and support the shift toward bilayer ETLs for improved performance stability [66–68].

SnO_2 has become a leading ETL for PSCs because of its higher electron mobility (~ 100–250 $cm^2|V^{-1}|\ s^{-1}$), excellent optical transparency, and better energy alignment with perovskite conduction bands. It also exhibits significantly lower photocatalytic activity compared to TiO_2, offering improved long-term stability [43, 69]. Recent experimental research shows progress in colloidal SnO_2 nanoparticle synthesis, which allows for low-temperature deposition (< 150 °C), critical for flexible substrates. Researchers have developed dopant-engineered SnO_2, including Li-, Sb-, or Nb-doped SnO_2 to reduce the deep trap densities and further boost conductivity. Additionally, SnO_2 with surface passivation using self-assembled monolayers (SAMs) or alkali halides (e.g., CsF) has dramatically improved open-circuit voltages in PSCs [70, 71]. On the simulation front, SnO_2 ETLs are analyzed with detailed modeling of nonparabolic conduction bands, especially for degenerately doped films where the effective mass and carrier concentration evolve with energy. These simulations are essential for understanding mobility degradation at high carrier densities and optimizing ETL thickness. Studies also compare SnO_2-perovskite interfacial recombination velocities, helping explain improved fill factors and long-term stability relative to TiO_2 [72].

ZnO has a higher electron mobility than both TiO_2 and SnO_2 (~ 200–300 $cm^2|V^{-2}|\ s^{-1}$) and a wide bandgap (~ 3.3 eV), making it ideal for transparent optoelectronic applications. However, its Achilles' heel has been chemical instability in contact with perovskites, leading to unwanted interfacial reactions that degrade the active layer. Experimental advancements focus on stabilizing the ZnO interface through surface functionalization or incorporation of buffer layers (e.g., fullerene derivatives, MgO) to prevent direct contact with the perovskite. Doping with Al, Ga, or Mg can tune ZnO conduction band while improving film crystallinity and reducing defect densities. Studies also explore sol-gel processes and atomic layer deposition (ALD) for conformal and defect-tolerant ZnO layers [73, 74]. Simulations now play a vital role in guiding ZnO applications by analyzing band alignment, built-in potential, and interface recombination dynamics. Hybrid ETLs like ZnO graphene or ZnO/TiO_2 are modeled to assess how charge transport improves when ZnO high mobility is combined with a chemically inert buffer layer. ZnO role in UV photodetection and transparent electrodes is also being increasingly evaluated with multi-physics models [75, 76].

Table 2 summarizes the key physical, chemical, and simulation-related attributes of TiO_2, SnO_2, and ZnO. This comparative matrix highlights how each material performs in terms of electron mobility, energy alignment, UV stability, deposition temperature, and modeling focus, enabling a holistic evaluation of their suitability for different device architectures. The table also outlines their primary challenges, providing context for why hybrid or modified ETL systems are gaining traction in current research.

3.2 Fabrication techniques of low temperature processed ETLs

The methods of depositing low-temperature ETLs onto conductive substrates or directly onto the perovskite absorber in solar cells. Here, we highlight the key features of the most used approaches.

3.2.1 Solution process

The solution process is commonly employed to deposit low-temperature-processed ETLs, either through thermal decomposition of metal salt precursors or by direct synthesis of nanocrystals and nanocolloids (Fig. 3(a) [47, 82, 83]. In the thermal decomposition approach, a metal salt precursor is dissolved in a suitable solvent and deposited onto the substrate using techniques such as spin-coating or spray-coating. Therefore, the deposited films are then converted into the desired layers by thermal annealing. In the nanomaterial-based route, the crystallization of the oxide is decoupled from the film-formation step, allowing the nano-sized solution to be directly deposited through methods like spin-coating, slot-die coating, or ink-jet printing. Notably, slot-die coating and ink-jet printing offer significant potential for large-scale manufacturing of ETLs. The solution process has been widely adopted in fabricating low-temperature ETLs for high-performance planar perovskite solar cells, as it enables good crystallinity and minimizes film defects. However, factors such as ambient humidity and annealing temperature play a critical role in ensuring the preparation of high-quality films during the thermal decomposition process [84].

3.2.2 Atomic layer deposition process

ALD is a key technique for finely controlling film growth, widely used to fabricate compact, uniform, and conformal thin films in the semiconductor industry [85]. It allows precise control over film thickness and is suitable even for

Table 2 Comparative summary of trends in TiO_2, SnO_2 and ZnO

Property	TiO_2 [77, 78]	SnO_2 [69, 79]	ZnO [80, 81]
Electron mobility	Low (0.1–4.1 $cm^2\|V^{-1}\| s^{-1}$)	Moderate-High (100–250 $cm^2\|V^{-1}\| s^{-1}$)	High (200–300 $cm^2\|V^{-1}\| s^{-1}$)
UV stability	Poor (UV photocatalytic activity leads to degradation)	Good (chemically stable under UV)	Moderate (better than TiO_2 but prone to instability without passivation)
Processing temperature	High (≥450 °C, sintering often required)	Low (<200 °C, solution-processable)	Moderate (150–250 °C)
Deposition methods	Spray pyrolysis, sol-gel, ALD, hydrothermal growth	Solution-processing, ALD, chemical bath deposition, spin-coating, slot-die coating	Sol-gel, sputtering, chemical bath deposition, spin-coating
Material crystallinity	High crystallinity required for good conductivity; mesoporous structures widely used	Amorphous or nanocrystalline layers effective; good surface coverage at low temperature	Nanocrystalline or polycrystalline; prone to defect formation at grain boundaries
Band alignment	Moderate (OK with most perovskites but not optimal)	Excellent (close match with perovskite conduction band)	Slight mismatch with some perovskites
Simulation focus	Defects, mesoporosity, interface traps	Nonparabolicity, doping effects	Interface stability, passivation strategies
Major limitation	UV degradation, recombination, high processing cost	Deep-level defects, synthesis control	Interface reactivity with perovskites, chemical instability
Device performance impact	Historically dominant ETL in PSCs but UV instability limits long-term stability; lower efficiency in large-area devices	Currently the most promising ETL for high efficiency and scalable PSCs due to low-temperature processing, good stability, and excellent band alignment	High electron mobility can give good efficiencies, but chemical reactivity with perovskites causes stability issues unless properly passivated

growth on rough substrates. A single ALD cycle typically consists of four steps: (1) exposure of the first precursor in the reactor chamber to form a layer on the substrate; (2) purging of excess precursor and by-products; (3) exposure of the second precursor; and (4) removal of the excess second precursor and by-products. The ALD deposition process of ZnO is illustrated in (Fig. 3(b) [44]. Importantly, ALD is compatible with flexible substrates, and crystalline films can be obtained at relatively low growth temperatures. So far, ALD has been successfully applied in preparing low-temperature-processed ETLs such as TiO_2 [86], ZnO [87], and SnO_2 [88] for high-performance perovskite solar cells. However, ALD remains costly, time-consuming, and highly sensitive to substrate purity, which limits its suitability for scalable production.

3.2.3 Chemical bath deposition process

CBD is a widely used technique for depositing semiconductor layers, where substrates are immersed in dilute solutions containing metal ions and sources of hydroxide or sulfide ions, as shown in (Fig. 3(c)) [89]. It has been proven effective for preparing semiconductor layers in thin-film solar cells, such as CdS or Zn (S, O, OH) for Cu (In, Ga)Se_2 and Cu_2ZnSnS_4 [90]. More recently, CBD has also been employed to fabricate efficient ETLs such as TiO_2, ZnO, and SnO_2 for planar perovskite solar cells with an n-i-p structure [91]. This method is particularly attractive because it is compatible with low-temperature and large-scale processing, offering advantages such as low fabrication cost, ease of growth adaptation, and high reproducibility [84]. However, growth conditions including temperature, concentration, and pH of the solution play a critical role in determining the quality of the resulting thin films.

3.2.4 Other deposition processes

In addition to the deposition processes mentioned above, several other effective methods are available for preparing low-temperature-processed ETLs, depending on the physicochemical properties of the materials. For instance, electrochemical deposition (ED) is a common approach for producing high-quality thin films and has been successfully applied to TiO_2, ZnO, and SnO_2 ETLs in regular perovskite solar cells [92]. The ED technique offers the advantages of a simple and rapid deposition process, low-temperature preparation, and precise control over film quality. By adjusting parameters such as current density and deposition time, films with strong adhesion to the substrate can be achieved [36]. Additionally, physical deposition techniques such as magnetron sputtering (Fig. 3(d)) and electron-beam evaporation have also been employed for ETL fabrication [93].

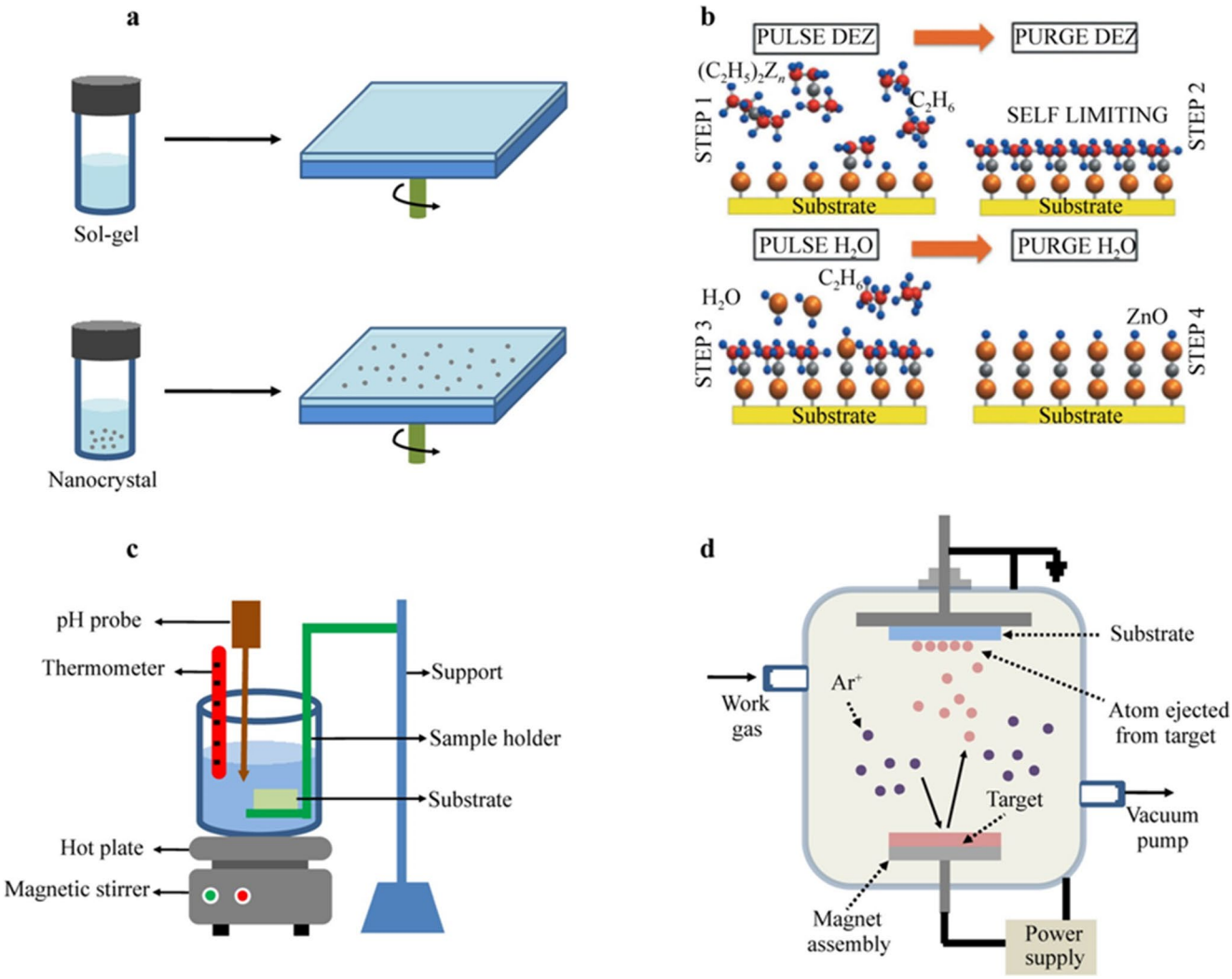

Fig. 3 Schematic illustration of typical deposition methods for ETLs: (**a**) solution processing, (**b**) atomic layer deposition for ZnO films, (**c**) chemical bath deposition, and (**d**) magnetron sputtering

These methods show great potential in flexible device applications since crystallization can occur during deposition, eliminating the need for post-annealing.

3.3 Titanium oxide (TiO_2)

TiO_2 is often used as an ETL in traditional PSCs owing to its chemical stability, superior charge transport characteristics, affordability, and simplicity of fabrication [94]. TiO_2 has a low refractive index ranging from 2.4 to 2.5 and a substantial band gap 3.2 eV for anatase, 3.1 eV for brookite, and 3.0 eV for rutile. The CBM is approximately − 4.1 eV, marginally lower than the LUMO level of perovskite, facilitating effective electron transport from the perovskite layer to the TiO_2 ETL. Conversely, the VBM is significantly deep, providing exceptional hole blocking capability. The ETL of TiO_2 may be categorized as a mesoporous layer and a dense layer of TiO_2 [78]. Mesoporous TiO_2 facilitates the development of perovskite crystals, but dense TiO_2 is crucial for electron transport. The TiO_2 film typically requires calcination at temperatures over 400 °C to eliminate the organic binder (e.g., ethyl cellulose) and provide a porous structure that enhances transport capabilities; however, this process is detrimental to the deployment of the device in flexible configurations. A low-temperature method for the fabrication of nanostructured TiO_2 films is regarded as a technical advancement [95].

3.3.1 TiO_2 displaying diverse morphologies

The morphology of TiO_2 is greatly affected by its manufacturing method, which in turn dramatically influences the performance of perovskite solar cells. The morphology and dimensions of nanomaterials are closely associated with the

specific surface area and pore size of the membrane, hence affecting the device's efficacy. Lee et al. used TiO_2 nanoparticles measuring 25 nm and 41 nm as the mesoporous layer by spin coating mp-TiO_2 [96]. The enlarged dimensions of TiO_2 nanoparticles led to an augmented total pore volume and average pore diameter, hence enhancing perovskite penetration, and diminishing electron transport resistance. Small TiO_2 nanoparticles have a significant specific surface area, enabling the injection of photoelectrons. Adjusting the thickness resulted in PCEs of 18.03% for 25 nm and 18.72% for 41 nm, respectively. Liu et al. used commercial TiO_2 nanoparticles, with a diameter of 6 nm, to construct a dense ETL by spin coating, in conjunction with the creation of the mesoporous layer. The small size of the TiO_2 nanoparticles is tightly clustered, perhaps obstructing the perovskite from infiltrating the TiO_2 ETL. It may also provide a rough surface to enhance wettability and facilitate the nucleation and growth of perovskite. The PCE of 11.0% was attained by thickness optimization [97].

Well-aligned and carefully arranged nanoarray structures nanorods, nanowires, nanotubes may provide direct paths for efficient charge transfer and improve the penetration of perovskites compared to nanoparticles. The porous TiO_2 nanorod array developed by Yang et al. used Pulsed laser deposition as the ETL in perovskite solar cells, with a PCE of 14.1%. The resulting anatase TiO_2 nanostructures markedly increase the contact area between the TiO_2 layer and the perovskite layer, exhibiting enhanced electron-hole pair separation and electron extraction efficiency at the interface (Fig. 4). Wu et al. fabricated an amorphous titanium oxide nanowire (Am-TNW) thin film to function as an ETL for PSC via a low-temperature (< 150 °C) solution method. The Am-TNW thin film needs no annealing treatment and has exceptional transmittance. It may be next to the perovskite layer, promoting perovskite penetration and effectively reducing charge recombination. The device attained an average PCE of 18.3% [99]. Titanium dioxide nanotube arrays were fabricated using electrochemical anodization on a titanium substrate and used in PSCs devoid of hole transport materials. The optical band gap and conductivity of the material fluctuated with the structural length of the TiO_2 nanotube, achieving an optimal PCE of 3.64% at a tube length of around 9.4 μm. Additionally, Chen et al. constructed a three-dimensional flower-like TiO_2 nano-array layer, including one-dimensional anatase TiO_2 nanorods on the FTO substrate, using a low-temperature 80 °C chemical bath deposition method to replace the traditional mesoporous TiO_2 layer. The 3D flower-shaped TiO_2 nano-arrays significantly impede charge recombination and improve light harvesting efficiency (LHE), which increases with extended chemical bath deposition reaction time of the nano-arrays. The device achieves a maximum PCE of 15.71% with notable repeatability and little hysteresis [100].

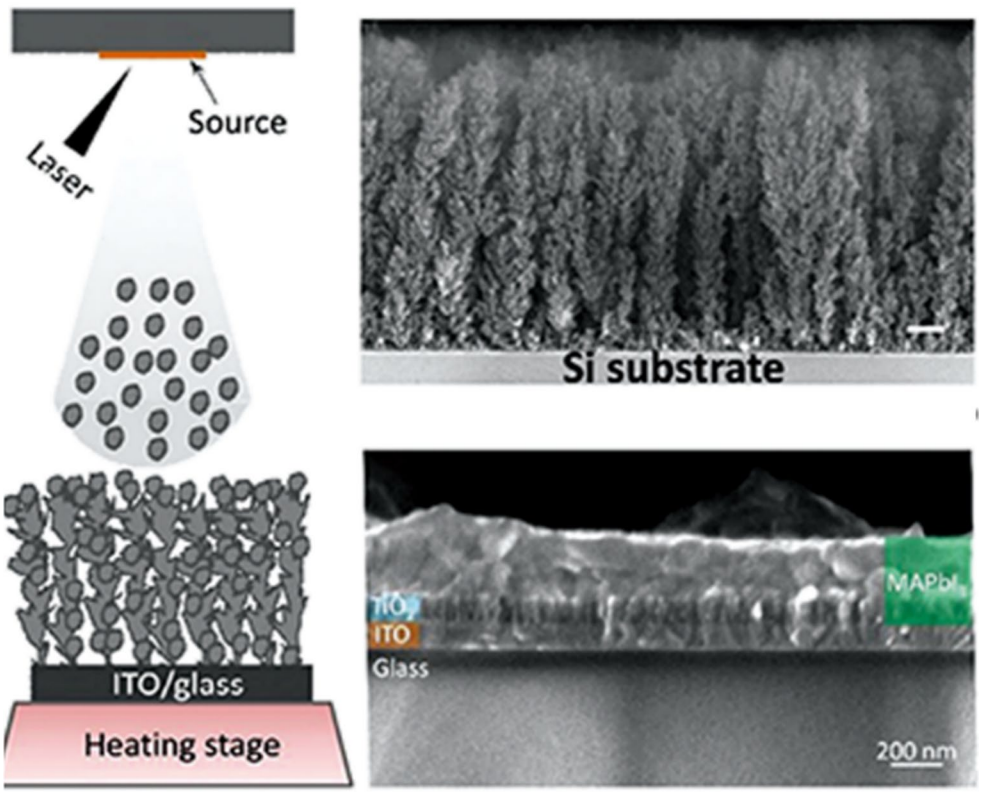

Fig. 4 The growth process of TiO_2 nanorod arrays using pulsed laser deposition (PLD) is shown in a schematic picture. SEM photographs of TiO_2 nanorods formed on silicon substrates by PLD at ambient temperature and cross-sectional SEM images of TiO_2 nanostructures produced on ITO glass substrates by PLD at 300 °C are also shown [98]. Copyright 2016 Royal Society of Chemistry.

3.3.2 TiO_2 element doping and interface modification

Device performance is affected by TiO_2 intrinsic defects include low valence Ti^{3+} ions and oxygen vacancies. Elemental doping and surface modification might improve material qualities and lower charge recombination in devices. With the main aim of constructing an interface structure that enables quick carrier transfer and inhibits recombination, surface modification is a useful method for changing carrier dynamics at the interface. An efficient modification approach to improve photovoltaic performance and reduce hysteresis in PSCs is the passivation of surface trap states in the TiO_2 and perovskite layers. Using $TiCl_4$ treatment, Tan et al. produced TiO_2 chlorine-modified colloidal nanocrystalline films [101]. Interfacial Cl atoms may reduce charge recombination at the interface by preventing the development of surface deep trap states, hence improving interface binding. With TiO_2-Cl, the small area device's 0.049 cm^2 PCE is 20.1%; the PCE of the big area device 1.1 cm^2 is 19.5%, thereby indicating good stability. Han et al. synthesized an 18.9% PCE device by combining TiO_2 with a bifunctional 4-picolinic acid (4-PA) self-assembled monolayer (SAM) [102]. Little hysteresis was detected when 4-PA treatment of TiO_2 improved the grain size of $MAPbI_3$, effectively passivate the interface of UK3 perovskite, and optimally transmit electrons and holes. Shen et al. showed on the surface of mesoporous TiO_2 film a modified layer of ultra-thin graphene quantum dots (QGD). While lowering contact resistance at the perovskite/mesoporous TiO_2 interface, the GQD incorporated into the mesoporous TiO_2 film improves electron extraction and transmission. From 18.57% to 20.45% the photoelectric conversion efficiency of the device rose [103]. TiO_2 helps to reduce charge recombination on the FTO surface and enable effective electron collecting. C60 helps to efficiently extract carriers from the perovskite layer; ZnO assures good energy level alignment between the TiO_2 layer and the C60 layer, thereby improving the open-circuit voltage. With a PCE of 18.63% the PSC using TiO_2/ZnO/C60 three-layer electron-transporting material attained (Fig. 5 (a)).

Introduction of dopant ions into the lattice sites of Ti^{4+} changes the band gap, energy level arrangement, carrier and (surface) trap state density and distribution, so improving photovoltaic performance, lowering hysteresis, and strengthening the stability of PSC. High-valence metal elements doping into the TiO_2 layer (n-type doping) may provide extra electrons, move the conduction band of the TiO_2 higher, enhance photoelectron injection process, and raise conductivity. Reduced trap state density, greater conductivity and electron mobility, and improved injection and extraction efficiency of photoelectrons indicate that the Nd-doped TiO_2 made by chemical bath deposition by Yin et al. enhances these parameters [106]. Better device stability and more than 19% PCE are obtained by the PSC with 1% Nb-doped TiO_2 although there are no surplus electrons in the dopant, the doping of comparable metal elements into the TiO_2 layer may modify the band gap, energy level arrangement, carrier mobility and trap state density. This

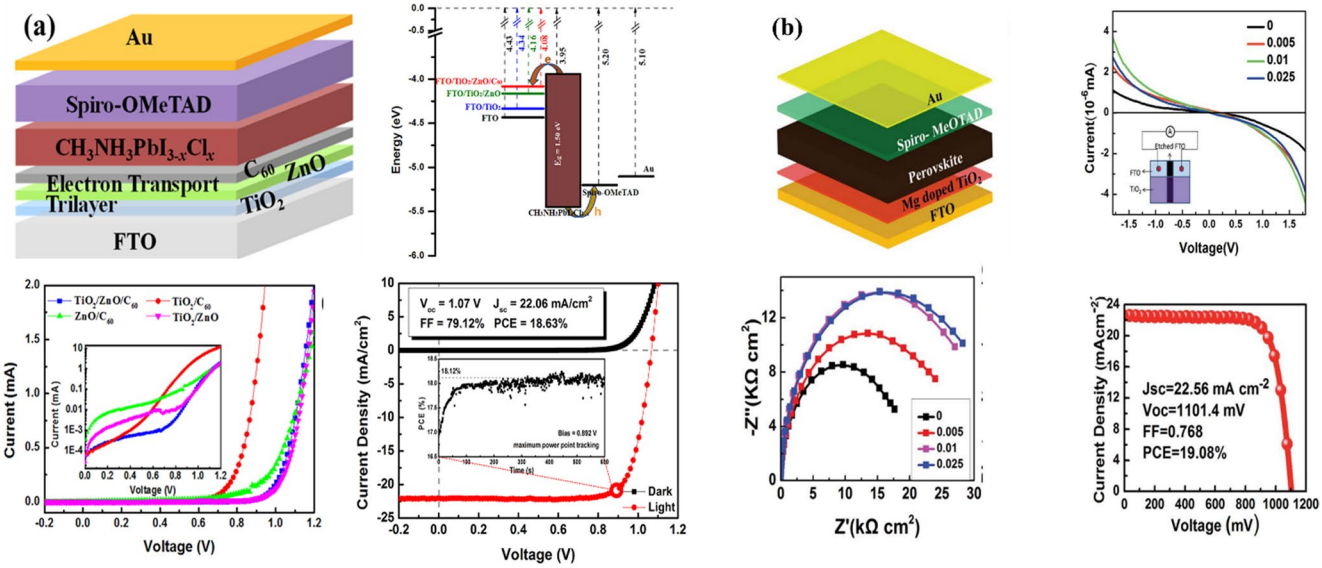

Fig. 5 (**a**) Schematic representation of the device architecture and energy level configuration for the TiO_2/ZnO/C60 electron transport trilayer planar PSC, J-V characteristics of PSCs utilizing four distinct compound ETLs, and the optimal PSC performance (the inset illustrates maximum power point tracking over 10 min, yielding a stabilized PCE of 18.12% at 0.892 V) [104]. Copyright 2018 American Chemical Society. (**b**) The device architecture using Mg-doped TiO_2, conductivity measurement outcomes for films with varying Mg treatment concentrations (the inset illustrates the sample structure for this measurement), Nyquist plots at 700 mV, and J-V curves [105]. Copyright 2016 Royal Society of Chemistry.

will not produce the change in carrier density. Sn-doped TiO_2 nanorod arrays, for instance, may raise band gap and enhance electron mobility, thereby improving device efficiency relative to undoped ones [107]. While the doping of suitable low concentration can reduce the defects of the TiO_2 (oxygen vacancies, Ti^{3+} gaps, etc.), so improving the conductivity, the doping of low-valent metal elements into the TiO_2 layer (p-type doping) usually results in the decrease of conductivity due of the decrease of electron density. By lowering the resistivity and moving the Fermi level higher, the TiO_2 layer doped with low concentration of Y and Mg may minimize the trap state density, thereby boosting the capacity to transport electrons and block holes. The device gets PCE of 19.3% and 19.08% respectively **(**Fig. 5 **(b))** [107, 108], and displays greater open circuit voltage and fill factor. Usually found in the lattice gap, the metal ions with lower radius are doped into the TiO_2 layer. Li-doped TiO_2 may, for instance, lower the electron trap density and increase conductivity. From 14.2% to 17.1% the photoelectric conversion efficiency of PSC based on Li-doped TiO_2 increases the hysteresis is negligible [108].

3.3.3 Low temperature manufacturing TiO_2

Cost-effective and flexible devices are incompatible with the high temperature manufacturing method of TiO_2. Many researchers have lately done significant study on the low-temperature manufacturing process of TiO_2 for flexible electronics. Kim et al. fabricated mesoporous TiO_2 as the ETL in high-efficiency PSCs using the reactive ion etching (RIE) technique instead of the conventional high-temperature annealing method. While the flexible device reached a PCE of 17.29%, the RIE-mp-TiO_2 showed improved electron extraction capacity and J-V hysteresis [109]. You et al. created TiO_2 nano-sols in acidic aqueous solution, Using the sol-gel method, then dispersed the dried TiO_2 nanoparticles in many solvents, then spin-coated and low-temperature annealed to produce the ETL. A homogeneous and hydrophilic TiO_2 ETL was created by using N, N-dimethylformamide (DMF) as a solvent, therefore reaching a PCE of 15.8% in the flexible device, which also showed good mechanical stability [110]. Xie et al. used a TiO_2/SnO_2 thin film created at a low temperature of 150 °C as the ETL in perovskite solar cells. They found a notable driving force for electron extraction at the SnO_2/perovskite interface, and a defect-free physical contact was created at the TiO_2/FTO interface. The bilayer thin film showed good hole blocking and effective electron extraction. With a maximum PCE of 18.85%, the device much outperforms the TiO_2-based device's PCE, which makes it very interesting for flexible PSC [111].

3.4 Tin(IV) oxide (SnO_2)

SnO_2 is regarded as a promising ETL material owing to its extensive band gap (conduction band minimum: −4.2 to −4.5 eV, band gap: 3.5 to 4.0 eV), low refractive index less than 2, high electron mobility approximately 250 $cm^2|V^{-1}|s^{-1}$, and appropriate energy band structure, which facilitates efficient electron extraction and transport, mitigates charge accumulation and recombination losses, and eradicates *J-V* hysteresis in planar PSCs [112].

3.4.1 SnO_2 exhibiting various morphologies

Baena et al. used ALD to fabricate a 15 nm thick, pinhole-free, dense layer of SnO_2 for application in a planar PSC. The film demonstrates extensive coverage and superior electron extraction capability, while the device displays high and steady current density with a PCE over 18%. Hagfeldt et al. fabricated a high-quality SnO_2 ETL using spin coating and chemical bath deposition (SC-CBD) for use in a planar PSC, achieving a high fill factor, effective hole blocking capability, enhanced stability, and reduced hysteresis, with a PCE approaching 21% (Fig. 6 (a)) [113]. Ke et al. fabricated a thick, thin film of SnO_2 using spin-coating a precursor solution of $SnCl_2{\cdot}2H_2O$ at ambient temperature. The thin film exhibits a smooth surface, high transmittance, effective electron extraction, and hole blocking capabilities, resulting in the device achieving an optimal PCE of 17.21% (Fig. 6 **(b))** [114]. Jiang et al. applied a spin-coating technique to deposit a solution of diminutive SnO_2 nanoparticles onto an ITO substrate, resulting in a pinhole-free, dense SnO_2 layer intended for a planar perovskite solar cell. The increased crystallinity of the SnO_2 nanoparticles facilitates a reduction in the density of defect states in SnO_2, resulting in a device with a PCE of 19.9% devoid of hysteresis. Li et al. fabricated a mesoporous SnO_2 film with large SnO_2 nanoparticles for mesoporous perovskite solar cells, achieving a PCE of 6.5% by optimization of the SnO_2 film thickness. Following the treatment of the SnO_2 film's surface with $TiCl_4$ aqueous solution, its PCE rose to 10.18% [115].

SnO_2 ETL preparation in PSCs has been described using a variety of approaches. By spin-coating a $SnCl_2$:$2H_2O$ precursor made at an ambient temperature and then thermal annealing it at 180 °C, Fang et al. implemented a low-temperature solution-based method to incorporate a SnO_2 ETL in PSCs. They achieved this by applying a $SnCl_2$:$2H_2O$ precursor onto the cells via spin-coating at room temperature, followed by thermal annealing at 180 °C. This novel strategy presents a substitute for conventional high-temperature manufacturing techniques used for SnO_2 ETLs, offering numerous advantages: such as (1), the utilization

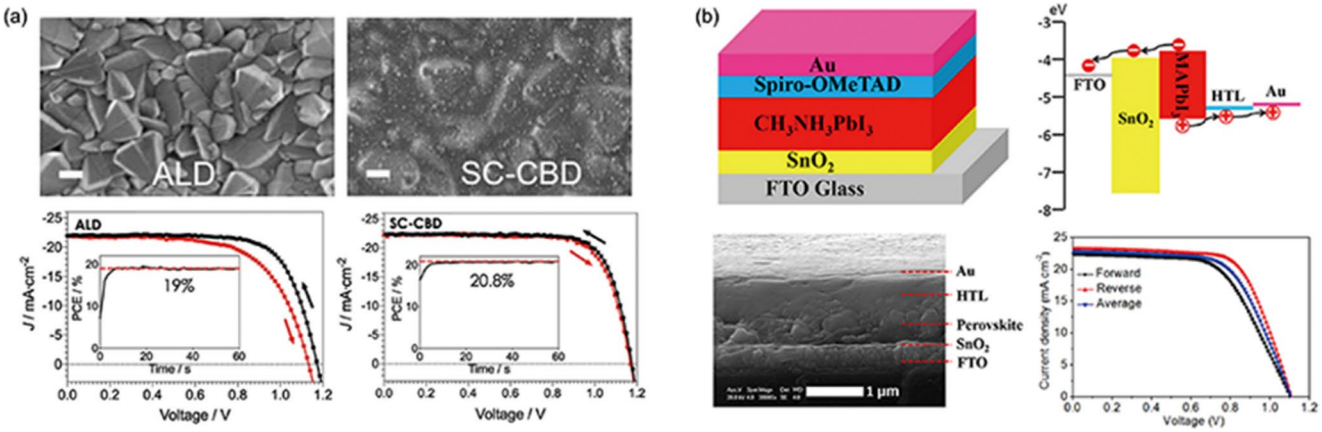

Fig. 6 (**a**) Presents SEM images and J-V curves with the inset showing maximum power point tracking for SnO_2 layers produced by atomic layer deposition, spin coating, and chemical bath deposition scale bars are 200 nm [8]. Copyright 2016 Royal Society of Chemistry. (**b**) Device architecture, energy level arrangement, cross-sectional SEM images, and J-V curve using spin-coated SnO_2 ETL [116]. Copyright 2015 American Chemical Society.

of a low-temperature solution-processed SnO_2 ETL method results in decreased energy consumption in comparison to high-temperature processes, hence enhancing its environmental sustainability and cost-efficiency [117]. (2), through the optimization of metal precursors concentration and deposition conditions, a polished In_2S_3 film was achieved, resulting in enhanced efficiency in the extraction and transportation of electrons compared to TiO_2 ETLs [118]. (3), the low-temperature solution-processed SnO_2 ETL approach offers a practical benefit in terms of efficiency and scalability due to its simplicity and fast processing, which may be completed in minutes [119]. (4), PSCs that utilize the low-temperature processed SnO_2 ETL demonstrated superior stability when compared to devices based on TiO_2. This suggests that the long-term performance and durability of the PSCs were improved [120]. (5), the low-temperature processed SnO_2 ETL has efficient charge transport due to its excellent charge mobility, broader bandgap, and advantageous band energy alignment. This leads to increased PCEs in PSCs [119].

A PCE of 17.21% was attained by SnO_2-based devices, which may be ascribed to the suitable characteristics of nanocrystalline SnO_2 material [121]. The term "suitable characteristics" of nanocrystalline SnO_2 material generally refers to specific material qualities that render it optimal for diverse purposes. Such as band Gap, SnO_2 has a broad band gap, usually measured at 3.6 eV or above. This property has a significant impact on the optical and electrical characteristics of SnO_2, making it well-suited for applications such as gas sensors and varistors [122]. The capacity to modify the electrical characteristics of SnO_2, such as its conductivity and the mobility of its charge carriers, increases its usefulness in various applications such as catalysts, resistors, and electrochemical devices [122]. The microstructural properties of nanocrystalline SnO_2, such as grain size and surface composition, have a substantial impact on its performance in gas sensors and other electronic devices [122].

The electronic structure of SnO_2 is affected by changes in its surface composition, specifically as it transitions from stoichiometric to reduced surfaces. This alteration results in the production of surface states and a decrease in the work function, making SnO_2 very suitable for gas sensor applications [122].The sensitivity of nanocrystalline SnO_2 particles to gases such as hydrogen is influenced by the thickness of the space charge layer. Improved performance is observed when the grain size is approximately twice the depth of the space charge layer [122]. To create SnO_2 ETLs in PSCs, Hagfeldt and coworkers used a combination of spin-coating $SnCl_4{\cdot}5H_2O$ precursor and a chemical bath $SnCl_2{\cdot}2H_2O$ solution with additives post-treatment approach. This method increased interest in using the alternative wide bandgap oxide. Their findings showed that using SnO_2 as the ETL produced a significant open-circuit voltage and a high, stable PCE of close to 21% and (V_{oc}) of 1.21 V [123]. Another example is the low temperature 150 °C solution processed SnO_2 Nanoparticles produced from the SnO_2 colloid precursor serve as the ETL in PSCs. This use of the ETL exhibited PCE of up to 20.54% in PSCs with improved charge extraction [124]. Wang and coworkers have described a Sol-gel wet chemical method for fabricating crystalline SnO_2 ETL below 80 °C. During refluxing, adding ambient O_2 and H_2O significantly speeds up Sn^{2+} oxidation from Sn^{2+} to Sn^{4+} and the hydrolysis of the $SnCl_2{\cdot}2H_2O$ alcohol solution. After ageing at room temperature, ultra-small SnO_2 nanoparticles less than 5 nm in diameter are produced, which produced PSCs with a PCE of 19.2% [42].

Correa-Baena et al. have developed a low temperature 120 °C ALD technique for the fabrication of devices using

SnO_2 as the ETL. They were the first to document a SnO_2 ETL that had a barrier-free energetic arrangement and produced a nearly hysteresis-free PCE of over 18% with a high V_{OC} of up to 1.19 V [125]. Shin et al. also showed that ALD is a potent method for depositing high-quality SnO_2 film as the ETL in PSCs. Kiani et at. In their research findings demonstrated that SnO_2 ETLs had superior performance compared to conventional materials such as TiO_2. This was attributed to their enhanced electron extraction and transport efficiency, resulting in increased performance of solar devices and higher PCEs. SnO_2-based PSCs exhibited superior stability and endurance when compared to devices that employed alternative ETL materials. This highlights the promise of SnO_2-based PSCs for long-term reliability and high performance in solar cell applications. The introduction of a novel and efficient method for fabricating SnO_2 ETL in high-performance PSCs was achieved by combining spin-coating with a chemical bath post-treatment approach. This creative approach encourages future study and optimization of the process [126].

Zafoschnig et al. discovered that after post-annealing at high temperatures 300 °C, ALD SnO_2 films had highly conductive leakage channels that had poor hole blocking abilities [128], demonstrating the need of low temperature annealing for ALD SnO_2 films to achieve high PCE in PSCs [129]. Due to its great surface coverage and conformality [130], ALD-deposited SnO_2 has been extensively used in tandem solar applications. Figure 7 illustrates that the ALD-deposited SnO_2 functions as a buffer layer to mitigate sputter damage from the succeeding transparent conductive oxide layers necessary for the clear front contact. To enhance efficiency, a thin layer of fullerene (C60 or PCBM) ETL is often interposed between the perovskite and SnO_2 layers. This layer facilitates electron movement across the interface, reduces the density of trap states, and has shown the ability to passivate grain boundaries [131]. These innovations show how useful ALD may be as a deposition method for massive procedures to deposit SnO_2 ETLs for PSCs. Al_2O_3 and other passivation layers are often deposited using ALD in the crystalline silicon solar cell sector [132].

There are still a lot of problems that need to be resolved even though SnO_2 has gained recognition in the scientific community and is widely utilized as a standard ETL in PSCs. The differences in the characteristics of SnO_2 films formed from Sn(II) and Sn(IV) salt precursors are among them, as is a full knowledge of the Cl residue from the

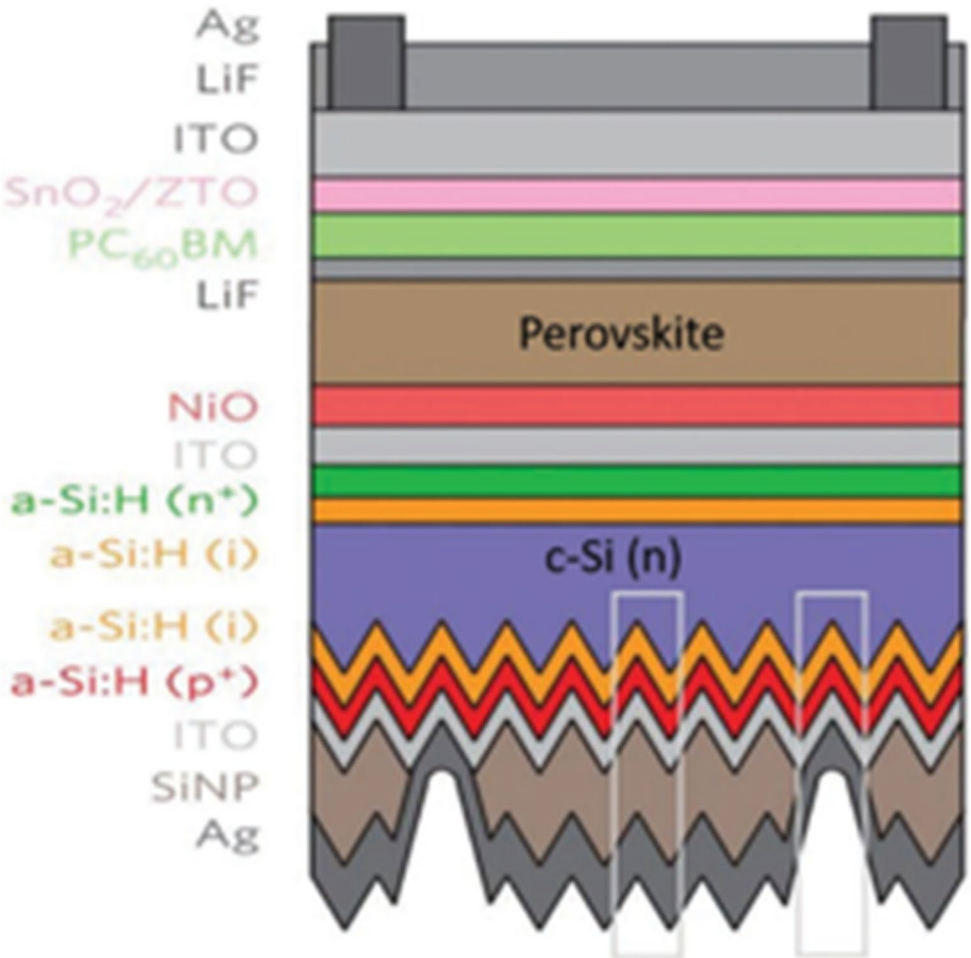

Fig. 7 Diagram of the silicon/perovskite tandem solar cell with ALD-deposited SnO_2 next to the PC60BM ETL layer [127]. Copyright 2017, Macmillan Pubhlishers Limited.

$SnCl_2 \cdot 2H_2O$ or $SnCl_4 \cdot 5H_2O$ precursor. Additionally, the difference between the dominant and favored crystal orientations ((110) and (200)) should be considered, because the crystal orientation can affect the mobility of charge carriers (electrons or holes) within the material. The presence of specific crystal planes may influence the ease with which charge carriers move through the lattice. In some cases, one orientation may exhibit higher carrier mobility than the other [133]. The colloidal synthesis methods used for SnO_2 nanoparticles may not offer the same level of accuracy and control over crystal orientation as the chloride preparation route. Although colloidal methods are simple and scalable, the chloride preparation route is particularly notable for its capacity to customize crystal orientations, improve charge carrier mobility, and optimize material properties for specific applications. Therefore, it is the preferred choice when precise control over crystal orientation and charge carrier mobility is essential [134].

Fluoride migration and consequent over doping of the SnO_2 ETL have, too, made it difficult for SnO_2 to sinter at higher temperatures on FTO substrates. The detrimental effect of fluorine doping is commonly used to enhance the electrical conductivity of tin oxide. However, excessive fluoride migration and over-doping can lead to increased carrier concentration beyond the optimal level. This may result in a decrease in carrier mobility, a phenomenon known as carrier freeze-out, which can hinder the overall electrical performance of the mater [135]. This has had an influence on device topologies using mesoporous SnO_2 because sintering the nanocrystal-line mesoporous electrode is necessary [136]. The negative impact of fluoride migration and excessive doping on SnO_2, specifically in the context of SnO_2 ETLs on FTO substrates, has resulted in difficulties in sintering at elevated temperatures due to the excessive movement of fluoride. Fluorine doping is frequently employed to improve the electrical conductivity of tin oxide. However, excessive doping can cause the carrier concentration to exceed the ideal threshold, resulting in decreased carrier mobility and a phenomenon referred to as "carrier freeze-out." This can ultimately impede the electrical performance of the material [137]. The excessive doping of fluorine in SnO_2 has had a significant impact on device topologies that use mesoporous SnO_2. This has led to the need for sintering the nanocrystalline mesoporous electrode. The transition of SnO_2 from facilitating low-temperature sintering to encountering difficulties caused by excessive fluorine doping emphasizes the need for careful optimization of SnO_2 characteristics for individual applications [138]. Concerning the mesoporosity of sintered SnO_2, the sintering process generally entails the compaction of particles to create a cohesive solid structure. Although sintering could decrease the porosity of the material, it is still feasible to maintain a certain degree of mesoporosity based on the sintering circumstances and the original structure of the material. Thus, sintered SnO_2 can retain mesoporous properties to a certain degree, however the level of mesoporosity may differ depending on the precise sintering settings and the desired application demands [139].

3.4.2 Modification of surface and doping of elements in SnO_2

SnO_2 has been shown to be an optimal material for ETLs, exhibiting superior performance. Nonetheless, the intrinsic flaws of SnO_2 film such as tin vacancies and oxygen vacancies lead to significant interface recombination at the SnO_2/perovskite junction, resulting in decreased open circuit voltage and fill factor [140]. The efficacy of SnO_2 devices may be enhanced by interface modification. Hao and colleagues used KCl to passivate the flaws at the SnO_2/perovskite interface, enhancing the device's efficiency and stability while mitigating the hysteresis problem. A planar PSC achieved a PCE of 20.5% [141]. Yang et al. introduced self-assembled monolayers (SAMs) with diverse functional groups onto the SnO_2 surface to facilitate multiple chemical interactions with the perovskite layer, therefore reducing the density of trap states and enhancing interfacial charge transfer [142]. The device surface, modified with a 4-picolinic acid self-assembled monolayer, attained a PCE of 18.8%. Xie et al. enhanced the electronic characteristics of SnO_2 films by using a tiny quantity of graphene quantum dots [143]. The photogenerated electrons in the GQDs are transferred to the conduction band of SnO_2, thereby filling electron traps, augmenting electron density, and enhancing SnO_2 conductivity. This process facilitates improved electron extraction rates and diminishes interface charge recombination. The device achieves an optimal PCE of 20.23% **(**Fig. 8**).**

Doping elements is a significant method to enhance the performance of SnO_2 devices. Doped SnO_2 enhances conductivity and elevates the Fermi level, facilitating interface charge transfer and diminishing interface charge recombination. The current investigation focuses on the impact of doping metals, including Li, Mg, Zn, Al, Y, Ga, La, Mo, Nb, and Sb, into SnO_2 as dopants on device performance [144–152]. Anaraki et al. synthesized a 5% Nb-doped SnO_2 ETL using CBD for use in a planar PSC. The device exhibits reduced series resistance, increased short-circuit current, and an enhanced fill factor, attaining an ideal PCE of 20.5% with improved repeatability. Xu et al. included La into the SnO_2 precursor solution to mitigate the aggregation of SnO_2 crystals and achieve a homogeneous surface devoid of pinholes. The La-doped SnO_2 significantly decreased the energy band offset, enhanced conductivity, and transparency, and facilitated charge injection and transfer. The open-circuit

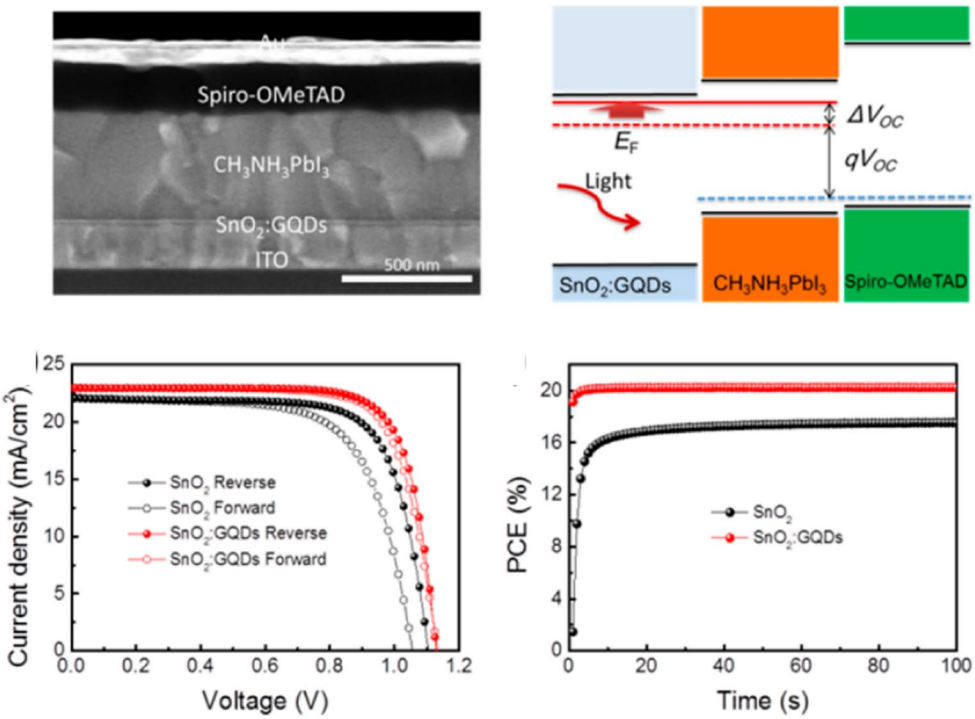

Fig. 8 Shows a cross-sectional SEM picture of PSCs including GQD-modified SnO_2, a schematic illustrating hot electron transfer from GQD to SnO_2 under illumination, the J-V curve for devices using SnO_2 and SnO_2:GQD, and the results of stability tests [143]. Copyright 2017 American Chemical Society.

voltage measured was 1.11 V, and the PCE recorded was 17.08% [153]. Song et al. synthesized Y-doped SnO_2 by the solvothermal process, resulting in a more compatible energy level structure with the perovskite layer, enhancing carrier transport and achieving an optimal PCE of 20.71%, with minimal hysteresis [154]. Furthermore, Hui et al. doped the SnO_2 film, synthesized at low temperature, with red carbon quantum dots (RCQ) abundant in carboxylic acid and hydroxyl groups. They discovered that the RCQ-doped SnO_2 film exhibited superior electron mobility and enhanced hydrophilicity, facilitating the passivation of traps and defects at the TiO_2 perovskite interface and promoting the development of highly crystalline perovskite films [155]. The RCQ-doped SnO_2 device attains a peak PCE of 22.77% and demonstrates remarkable humidity stability. The persistent endeavors of scientists have enhanced the photoelectric conversion efficiency of SnO_2 planar PSCs to above 23%, indicating significant development potential [156].

3.4.3 SnO_2 synthesized at low temperatures

SnO_2 is extensively used in flexible PSCs owing to its low crystallization temperature. Liu et al. synthesized a highly crystalline SnO_2 ETL devoid of ligands at a low temperature 100 °C utilizing spin coating and hydrothermal treatment for flexible PSCs. They discovered that hydrothermal treatment facilitated the thorough elimination of organic active agents from the surface of SnO_2 nanoparticles via hot water vapor, while also enhancing crystallization through the elevated vapor pressure of water, resulting in high-quality SnO_2. The device attains a peak PCE of 18.09% and exhibits commendable environmental stability, retaining over 90% of the original efficiency after 1000 bends. Chen et al. produced a high-quality SnO_2 ETL for flexible devices by a low-temperature 120 °C production method and examined the influence of various solvents and deionized water on the crystallization process of SnO_2. A continuous, pinhole-free, compact, and highly crystalline SnO_2 film may be synthesized using a solvent composed of 5% water and butanol. The device has an ideal PCE of 18% and demonstrates commendable mechanical stability [157]. Zhong et al. used a SnO_2 film synthesized at a low temperature 140 °C in the flexible PSC and included a hydroxyl-modified fullerene derivative (CPTA) layer at the SnO_2/$MAPbI_3$ interface, enhancing conductivity and diminishing the interface barrier to optimize device performance. The device achieved a peak PCE of 18.36% and demonstrated commendable environmental stability and mechanical bending resilience [158].

3.5 Zinc oxide (ZnO)

Another popular ETL in PSCs is ZnO. ZnO has a comparable CBM (−4.3 eV, relative to the vacuum level) and broad bandgap (>3 eV) to TiO_2 and SnO. Compared to TiO_2 and SnO_2, ZnO has several benefits. The electron mobility of bulk ZnO crystals may reach 300 $cm^2\ V^{-1}s^{-1}$, that of ZnO thin films is >600 $cm^2|V^{-1}|\ s^{-1}$, and that of 1D materials is 1000 $cm^2|V^{-1}|\ s^{-1}$ [159]. Compared to TiO_2 and SnO_2, ZnO has less reports and applications as an ETL while having

these promising features. This might be caused by two things: (i) have a historically lower device efficiency which prevents efficient perovskite annealing and (ii) poor thermal stability [160]. The historical performance of electronic devices using ZnO as an ETM might have been lower compared to devices using TiO_2 or SnO_2. Device efficiency is a crucial factor in the adoption of materials for specific roles in electronic devices, such as solar cells or other optoelectronic applications.

The historical lower device efficiency and poor thermal stability of ZnO as an ETL in electronic devices, particularly in perovskite solar cells, have limited its widespread adoption. These drawbacks can be attributed to the following reasons [161]. ZnO has historically exhibited lower device efficiency compared to other ETLs like TiO_2 or SnO_2, which can hinder the overall performance of electronic devices. This lower efficiency may be due to challenges in achieving efficient perovskite annealing when using ZnO as an ETL, impacting the device's overall functionality and energy conversion efficiency [161]. Another significant drawback of ZnO is its poor thermal stability, which can lead to degradation or performance issues in electronic devices, especially under high-temperature operating conditions. The lack of robust thermal stability in ZnO-based devices can limit their long-term reliability and operational efficiency, making them less favorable for certain applications [161]. If ZnO-based devices historically exhibited lower efficiency, it could have led to a preference for TiO_2 or SnO_2 in certain applications. The efficient perovskite annealing suggests that ZnO might face challenges in supporting the processing conditions required for perovskite solar cells. Efficient perovskite annealing is essential for achieving high-quality perovskite layers, and if ZnO is less effective in supporting this process, it could contribute to its lower adoption in such applications [160]. As an efficient ETL in p-i-n devices, ZnO layers formed from synthetic nanoparticles have been shown to be more stable than organic ETLs [162].

3.5.1 ZnO exhibiting various morphologies

The elevated electron mobility and low temperature processability of ZnO have resulted in the extensive use of homogeneous, dense ZnO films characterized by few flaws and pinholes in planar devices. Magnetron sputtering, ALD, and spray pyrolysis are efficient techniques for fabricating dense ZnO films with adjustable characteristics. For instance, Ngo et al. synthesized compact ZnO thin films by Spray pyrolysis under nitrogen gas flow results in high transmittance, excellent homogeneity, and comprehensive substrate covering [163]. The device attains a PCE of 12.7% and has commendable stability. Zheng et al. used combustion synthesis for the first preparation of high-quality ZnO thin films, which exhibit intrinsic passivation, high crystallinity, little carbon contamination, suitable energy level alignment, optimal shape, and excellent chemical compatibility with perovskite layers [164]. Devices using combustion synthesis ZnO thin films may get a PCE of 17% to 20% (Fig. 9(a)) [165]. Zhang et al. synthesized extremely crystalline and ultra-uniform ZnO nanoparticles of varying sizes using the solvothermal method [166]. The dimensions of the nanoparticles influence the filling and contact area of perovskite, the electron injection efficiency at the ZnO-perovskite interface, and the charge recombination capacity. The device using a 40 nm ZnO nanoparticle mesoporous layer attains an optimal PCE of 15.92%.

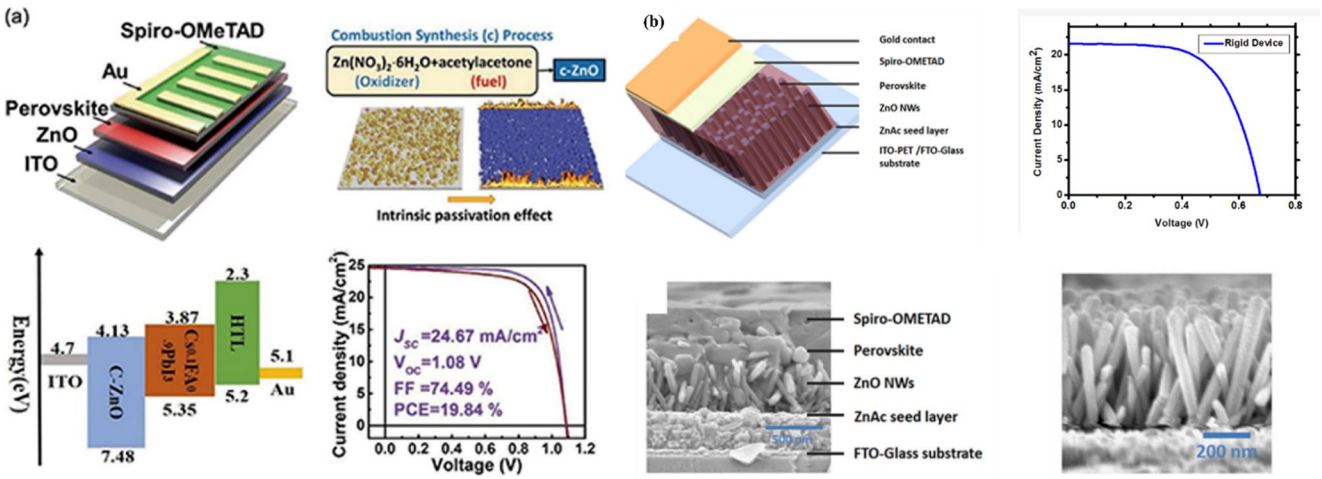

Fig. 9 (**a**) Device architecture including c-ZnO thin film, schematic representation of combustion synthesis, organization of material energy levels, and J-V curve of the devices [167]. Copyright 2019 John Wiley & Sons. (**b**) Device architecture including a ZnO nanowire array, J-V curve, and cross-sectional SEM picture of the PSC, together with a cross-sectional SEM image of ZnO NW cultivated for 75 min [168]. Copyright 2016 MDPI.

Effective PSCs have employed ZnO thin films from various nanostructures because of the simple crystallization of ZnO, hence enabling the creation of different nanostructures. Unlike nanoparticles, one-dimensional ZnO nanostructures are single crystals that provide a direct channel for electron transport. While creating high-quality perovskite films on their surfaces, ZnO nanorods vertical structural arrangement increases the contact area with perovskite. Li et al. used the hydrothermal method to create ZnO nanorods as an ETL and heated the substrate before spin-coating the perovskite to improve the surface coverage, grain size, and crystallinity of the perovskite [169]. The PCE of the device is 10.34% upon thickness adjustment. The high aspect ratio of ZnO nanowires helps perovskite to penetrate and improves electron transport. Etgar et al. created ZnO nanowires for PSC by hydrothermal techniques, tailoring their length and diameter to reach PCE of 9.06% and 6.39% for rigid and flexible devices, respectively, showing exceptional stability (Fig. 9 (b)) [170]. Furthermore, Islavath et al. built vertically aligned three-dimensional (3D) ZnO nanowall arrays on transparent conductive substrates using a seed layer-assisted low-temperature solution growth approach for a hole-free perovskite solar cell. The shape of the ZnO nanostructure may be gradually changed from one-dimensional nanowires to three-dimensional nanowall arrays by changing the aluminum concentration in the seed layer. With a high device PCE of 2.56%, the highly aligned 3D ZnO nanowires have a huge surface area and a unique cage-like structure that promote electron transport. One-dimensional ZnO nanowires are then grown on the surface of three-dimensional ZnO nanowires, hence improving the ZnO/perovskite contact and raising the PCE of the device to 3.28% [171]. The section below elaborates more on the ZnO surface modification.

3.5.2 ZnO surface modification and element doping

Despite the notable improvement in the performance of devices using ZnO ETLs, the considerable interface recombination and instability of ZnO thin films hinder their future development. For example, the inherent imperfections of ZnO include zinc vacancies, oxygen vacancies, dangling bonds, and defects resulting from the sudden disruption of the ZnO crystal structure. The newly introduced defects during the solution fabrication process may provide additional recombination pathways and diminish device performance. The ZnO surface is alkaline and will deprotonate $CH_3NH_3^+$ upon contact with perovskite, resulting in the facile disintegration of the perovskite deposited on the ZnO surface after thermal treatment [172, 173]. Surface modification or elemental doping may provide a solution to this issue. Surface modification effectively reduces charge recombination. Coating the ZnO ETL with a wide band gap oxide may passivate the interface and enhance device performance. Using the ALD technique, Li et al. deposited an Al_2O_3 monolayer on ZnO nanorods, which effectively passivates interface defects and enhances carrier separation, thereby increasing the device's photoelectric conversion efficiency from 11.72% to 16.08% and mitigating the chemical instability caused by residual chemicals [174]. Block copolymers such as PCBM and polyethyleneimine, with a lower conduction band edge than ZnO, are used to modify the interface between ZnO and perovskite, hence inhibiting interfacial recombination (Fig. 10 (a)) [175]. Zhang et al. developed a perovskite solar cell using a ZnO-PCBM bilayer electron transport material, employing PCBM as an interfacial modification layer [176]. The ZnO layer may enhance the energy level configuration and boost carrier extraction efficiency; the PCBM layer may augment the thermal stability of the perovskite and reduce hysteresis. This PSC offers enhanced device performance relative to the PSC of a single-layer ETL.

Moreover, element doping serves as an excellent method to enhance charge recombination and elevate the quality of ZnO thin films. Metal dopants including Li, Na, K, Mg, Al, Sn, In, and Ni may mitigate surface defects in ZnO, enhancing electron mobility and elevating the Fermi level [84, 179–183]. The PSC of the K-doped ZnO ETL attained a PCE of 19.9%, exhibiting remarkable air stability and no hysteresis (Fig. 10 (b)) [184]. Currently, substantial advancements have been attained in the modification of ZnO thin films; nevertheless, issues related to long-term stability need more optimization and investigation, this will further be discussed in the ZnO synthesis section.

3.5.3 ZnO synthesized at low temperatures

Increasing attention has been paid lately on flexible devices made using low temperature methods. The development of flexible technologies is greatly influenced by the low temperature processability of ZnO thin films. For flexible devices, Liu et al. created ZnO nanoparticle films by spin-coating at temperatures below 100 °C, hence increasing the creation of low-temperature ZnO films in flexible applications with a PCE of 10.2% [185]. Jung et al. fabricated the ZnO ETL at a temperature under 100 °C for use in flexible electronics. By adjusting the ZnO layer thickness, the size and shape of $MAPbI_3$, and the remaining PbI_2 phase, the device attained a peak PCE of 12.34% and exhibited commendable mechanical stability [186]. Lim et al. fabricated ZnO thin films at low temperatures for flexible devices and incorporated a PEIE modification layer on the ZnO surface, which prevented the decomposition of the perovskite layer, enhanced the crystallinity of perovskite thin films, and

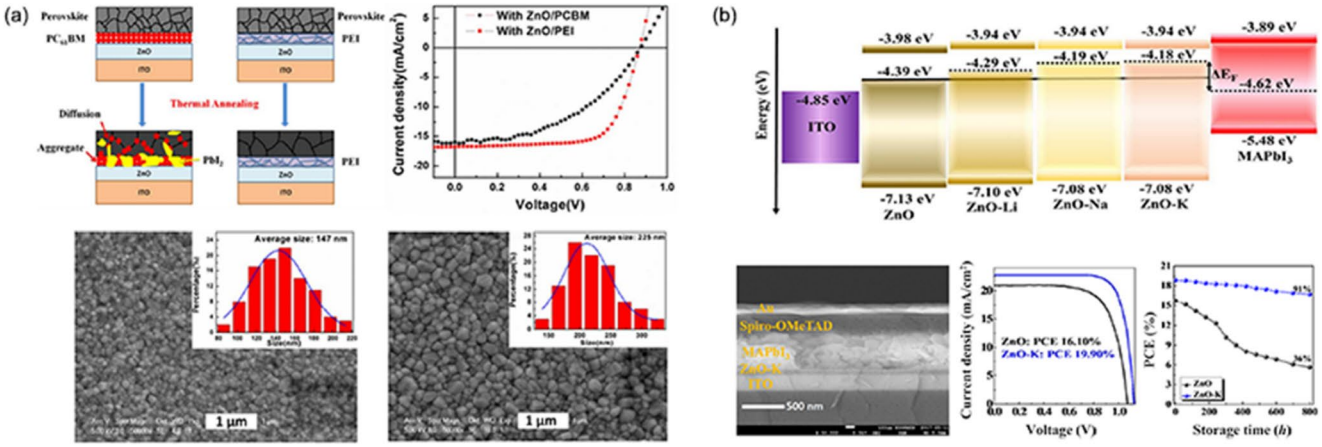

Fig. 10 (**a**) Depicts the schematics of perovskite growth on PC61BM-coated ZnO and PEI-coated ZnO during thermal annealing, the J-V curves of PSCs employing PC61BM-coated and PEI-coated ZnO, along with SEM images and grain size distribution of the perovskite film deposited on PEI-coated ZnO, both prior to and following thermal annealing at 100 °C for 1 h [177]. Copyright 2015 American Chemical Society. (**b**) Energy level configuration of devices employing ZnO and various element-doped ZnO, cross-sectional SEM imagery, J-V characteristics, and stability evaluation of devices utilizing K-ZnO (preserve unpackaged devices in a dark, ambient environment with relative humidity of 40% to 50% and temperature of 25 ± 3 °C) [178]. Copyright 2018 American Chemical Society.

lowered the electron transport barrier, resulting in a device efficiency of 11.9% PCE [165].

Table 3 highlights the key photovoltaic parameters V_{OC}, J_{SC}, FF, and PCE of PSCs employing various oxide based ETLs. By comparing device configurations that utilize common ETLs such as TiO_2, ZnO, SnO_2, and emerging alternatives like $ZnTiO_3$ and In_2S_3, the table offers a concise overview of how different ETL materials influence overall device performance. This comparative data is essential for identifying high-performing oxide ETLs and understanding the trade-offs between efficiency, voltage output, and current generation in various architectures. It serves as a valuable reference for researchers aiming to optimize ETL selection in the design of efficient and stable PSCs.

3.6 Large area modules and commercial prospects of inorganic ETLs

The transition from laboratory-scale solar cell prototypes to commercially viable large-area modules is a critical step toward the widespread adoption of photovoltaic technologies [210]. ETLs play a fundamental role in determining device stability, efficiency, and scalability. Inorganic ETLs have attracted significant attention due to their inherent thermal, chemical, and photostability compared to organic counterparts [211]. When solar modules are scaled up from small active areas (typically a few mm² or cm²) to large modules exceeding hundreds of cm², challenges such as uniform film deposition, charge extraction efficiency, and long-term operational stability become more pronounced. Inorganic ETLs such as TiO_2, SnO_2, and ZnO, owing to their robust physicochemical properties, offer promising solutions to these scale-up challenges [212–214]. Large-area module fabrication demands ETL materials that can be deposited uniformly over wide surfaces with high throughput, minimal cost, and compatibility with industrial processes such as roll-to-roll coating, spray pyrolysis, or slot-die coating [215, 216]. Inorganic ETLs are often amenable to these deposition methods, especially when engineered at the nanocrystalline level to improve surface coverage and reduce recombination losses [217]. Seen SnO_2 has emerged as a front-runner in perovskite solar modules due to its high electron mobility, wide bandgap, and low-temperature processability, making it suitable for flexible and tandem architectures. Furthermore, its compatibility with scalable techniques like chemical bath deposition and atomic layer deposition makes it particularly suited for industrial adoption [218].

From a commercial perspective, inorganic ETLs provide a cost-performance-stability trifecta that is essential for economic viability. Organic ETLs, while initially easier to process, tend to degrade faster under UV exposure and high humidity conditions often encountered in real-world installations [219]. Inorganic ETLs, by contrast, offer superior long-term stability, an essential requirement for solar modules expected to operate efficiently over 20–25 years. This reliability translates into lower maintenance costs and better return on investment for solar farms and residential systems, further reinforcing the commercial appeal of inorganic materials. Additionally, their environmental benignity and abundance (e.g. TiO_2 and ZnO) support sustainable manufacturing at scale, a key criterion for green energy technologies [117]. Another notable commercial prospect of inorganic ETLs lies in their integration into tandem solar cells especially perovskite/silicon tandems which are

Table 3 Photovoltaic parameters of PSCs based on different oxide ETLs [117]

Device configurations	ETL	V_{OC}[V]	J_{SC} [mA cm^{-2}]	FF	PCE [%]	long-term light stability	Ref.
FTO/SnO_2/$MAFAPbI_3$/Spiro-OMeTAD/Au	SnO_2	1.10	25.25	74.92	20.98	-	[187]
ITO/SnO_2/$FAPbI_3$/spiro-OMeTAD/Au	SnO_2	1.14	24.7	79.50	22.40	-	[188]
ITO/SnO_2/perovskite/spiro-OMeTAD/Au	SnO_2	1.13	25.0	77.03	22.37	-	[189]
FTO/SnO_2/$MAPbI_3$/spiro-OMeTAD/Au	b-SnO_2	1.11	23.3	0.67	17.2	-	[190]
FTO/c-TiO_2/paa-QD-SnO_2/$FAPbI_3$/Spiro-OMeTAD/Au	c-TiO_2/paa-QD-SnO_2	1.17	26.09	83.84	25.4	Sealed devices: ~95% of initial PCE retained after 100 h MPP tracking; ~70.5% retained after 700 h light-soak in open/unsealed condition.	[191]
FTO/c-TiO_2/mp-TiO_2/$FAPbI_3$/Spiro-OMeTAD/Au	c-TiO_2/mp-TiO_2	1.17	26.17	82.47	24.68	-	[192]
FTO/SnO_2/$(FAPbI_3)_{0.85}(MAPbBr_3)_{0.15}$/spiro-OMeTAD/Au	ALD-SnO_2	1.14	21.3	0.74	18.4	-	[125]
ITO/ZnO/$Cs_{0.1}FA_{0.9}PbI_3$/spiro-OMeTAD/Au	ZnO	1.08	24.7	0.74	19.8	-	[193]
FTO/$SrSnO_3$/$FA_{0.85}MA_{0.15}Pb(I_{0.85}Br_{0.15})_3$/spiro-OMeTAD/Au	$SrSnO_3$	1.13	22.3	0.67	16.9	-	[194]
FTO/In_2S_3/$MAPbI_3$/spiro-OMeTAD/Ag	In_2S_3	1.03	22.5	0.78	18.2	-	[195]
ITO/$InGaZnO_4$/$MAPbI_3$/spiro-OMeTAD/Ag	$InGaZnO_4$	1.14	22.7	0.67	17.4	-	[196]
ITO/$ZnTiO_3$/$Cs_{0.05}FA_{0.81}MA_{0.14}PbI_{2.55}Br_{0.45}$/sprio-OMeTAD/Au	$ZnTiO_3$	1.14	22.6	0.78	20.1	Holds ~ 90% of initial PCE after 100 h UV-soaking (365 nm, 8 mW cm^{-2})-UV-stability test reported in the paper.	[197]
FTO/SnS_2/$MAPbI_3$/spiro-OMeTAD/Au	SnS_2	0.95	23.7	0.60	13.6	-	[198]
FTO/c-TiO_2/TiO_2-B/$(FAPbI_3)_{1-x}(MAPbBr_3)_x$/spiro-OMeTAD/Au	TiO_2-B	1.05	24.9	0.72	18.8	-	[199]
FTO/c-TiO_2/$MAPbI_3$/spiro-OMeTAD/Au	c-TiO_2	1.10	23.4	0.77	20.0	>82% retention after 60 h of real-operating light test	[200]
FTO/c-TiO_2/mp-TiO_2/$FAPbI_3$/spiro-OMeTAD/Au	c-TiO_2/mp-TiO_2	1.13	25.9	0.82	24.0	-	[201]
ITO/SnO_2/$(FAPbI_3)_x(MAPbBr_3)_{1-x}$/spiro-OMeTAD/Au	c-SnO_2	1.09	24.9	0.76	20.5	-	[202]

Table 3 (continued)

Device configurations	ETL	V_{OC}[V]	J_{SC} [mA cm^{-2}]	FF	PCE [%]	long-term light stability	Ref.
FTO/r-TiO_2/$MAPbI_3$/spiro-OMeTAD/Au	r-TiO_2	1.17	23.3	0.77	20.9	-	[203]
FTO/c-TiO_2/mp-$SrTiO_3$/$MAPbI_{3-x}Cl_x$/spiro-OMeTAD/Au	c-TiO_2/mp-$SrTiO_3$	0.93	14.9	0.55	7.6	-	[204]
ITO/ZnO/$MAPbI_3$/spiro-OMeTAD/Ag	ZnO	1.03	20.4	0.75	15.7	-	[205]
FTO/TiO_2 coated WO_3/$MAPbI_3$/spiro-OMeTAD/Ag	TiO_2	0.87	17.0	0.76	11.2	-	[206]
FTO/c-TiO_2/ALDSnO_2/$(FAPbI_3)_{0.85}(MAPbBr_3)_{0.15}$/PTAA/Au	c-TiO_2/ALD SnO_2	1.13	22.7	78.0	20.0	-	[125]
FTO/In_2S_3/$CsPbIBr_2$/spiro-OMeTAD/Ag	In_2S_3	1.09	7.8	0.66	5.6	-	[207]
ITO/$ZrSnO_4$/$(FAPbI_3)_{0.95}(MAPbBr_3)_{0.05}$/spiro-OMeTAD/Au	$ZrSnO_4$	1.00	24.8	0.67	16.8	-	[208]
FTO/c-TiO_2/La-$BaSnO_3$/$MAPbI_3$/PTAA/Au	c-TiO_2	1.12	23.4	0.81	21.3	LBSO-based PSCs retained ~ 93% of initial PCE after 1000 h of full-sun illumination	[209]

rapidly emerging as the next frontier in photovoltaics due to their potential to exceed 30% PCE. Inorganic ETLs offer the necessary band alignment, minimal parasitic absorption, and interface stability required for these advanced architectures. Moreover, their mechanical and chemical robustness enables better yield during module lamination and encapsulation processes, which are critical for large-scale production [210].

Therefore, inorganic ETLs represent a pivotal technology enabler for the commercial success of large-area photovoltaic modules. Their compatibility with scalable fabrication, superior durability, and performance make them indispensable in the roadmap toward cost-effective, high-efficiency, and long-lasting solar energy systems [220]. As the photovoltaics industry continues to move toward terawatt-scale deployment, the role of inorganic ETLs will only become more central, not just in improving cell performance, but also in ensuring manufacturability, reliability, and economic competitiveness at scale [220].

3.7 ETLs impact on device stability

Despite being in the nascent phase of research, PSCs have yielded some favorable outcomes, with testing procedures meeting and exceeding significant stability test criteria as outlined by IEC standards, including IEC61215 for crystalline silicon and IEC61616 for thin-film modules. Despite these advancements, the commercialization of emerging photovoltaic technologies, specifically PSCs, is obstructed by challenges stemming from two sources: intrinsic factors related to the structural (chemistry/crystallinity) and interfacial stability of materials, and extrinsic factors concerning environmental conditions and the mitigation of external influences on the devices under evaluation. Numerous effective methodologies, such as compositional engineering [221], mixed-cation engineering [222], and dimensionality engineering, have been used to enhance the intrinsic stability of perovskites [223]. ETLs are crucial for the extrinsic stability of the device. ZnO, functioning as a Lewis base, is susceptible to MA deprotonation, leading to perovskite degradation, which may be exacerbated by the presence of surface hydroxyl groups and/or residual acetate ligands [224]. The interface issue may be mitigated by including a buffer layer and replacing MA with the less acidic FA cation or mixed cations, such as Cs, in perovskite materials [225]. The photocatalytic activity of TiO_2, caused by trapped holes at the TiO_2 and perovskite interface, leads to the degradation of $MAPbI_3$ into PbI_2 upon exposure to UV light [226]. A multifunctional fluorinated photopolymer coating may inhibit and mitigate UV damage [227]. Another drawback of using TiO_2 as an ETL is the relatively elevated trap density resulting from oxygen vacancies and interstitial defects in TiO_2. This results in device degradation. Chlorine doping in TiO_2-based devices effectively mitigates trap states and diminishes interfacial recombination [60]. Following sustained operation at the maximum power point under AM 1.5G illumination with a 420 nm cutoff UV filter, the chlorine modified TiO_2 device retained 90% of its initial

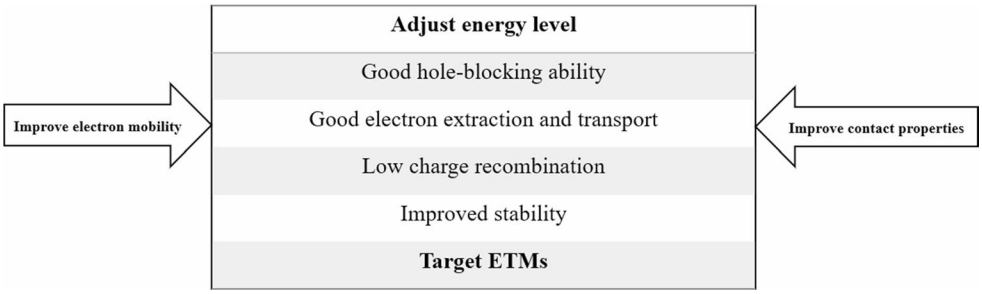

Fig. 11 Optimized modification role of the target ETLs

performance [228]. A chemical linker, 4-imidazole acetic acid hydrochloride, has been incorporated between the SnO_2 and perovskite layers. This molecule establishes a chemical linkage between SnO_2 and perovskite by an esterification process and electrostatic interaction, therefore eliminating interface defects and enhancing device stability in 40–60% relative humidity settings [229].

Kim et al. devised an interface passivation method by treating SnO_2 ETL with KOH, resulting in the formation of KBr that effectively passivates defects and reduces J-V hysteresis, hence enhancing the device's stability [141]. Figure 11 presents a consolidated overview of the optimized modification strategies applied to various inorganic ETLs in PSCs. This figure serves to illustrate how different doping methods, surface treatments, and interface engineering techniques have significantly enhanced the performance of ETLs especially SnO_2, TiO_2, and ZnO by improving charge transport, reducing recombination, and increasing device stability. Each segment of the figure visually encapsulates the role of these modifications in tailoring energy level alignment, boosting electron mobility, and mitigating interface defects. Collectively, these advancements underscore the critical role of materials engineering in pushing the boundaries of PSC efficiency and longevity.

3.7.1 Scalability

The practical integration of ETLs into PSCs demands more than just high laboratory-scale performance. For ETLs to be viable in real-world photovoltaic modules, they must meet stringent requirements in scalability, reproducibility, and long-term stability [230]. These three factors are deeply interlinked and collectively determine whether an ETL material can transition from research to industrial production. Even the most efficient lab-scale ETL can become a bottleneck if it fails in large-area coating uniformity, exhibits batch-to-batch variation, or degrades over time under environmental stressors [230]. Scalability refers to the ability to reproduce high-performance ETL films over large substrate areas using industrially compatible deposition techniques. While spin-coating remains the dominant method in research settings due to its ease and control over small areas, it is inherently non-scalable [231]. Industrial-scale manufacturing requires scalable techniques such as blade coating, slot-die coating, inkjet printing, or spray pyrolysis. In this context, the ETL must be chemically and physically compatible with these methods, exhibiting good wetting, film-forming properties, and rapid drying at low temperatures [231]. Inorganic ETLs like SnO_2 and ZnO, especially in colloidal or sol–gel form, show promise due to their tunable rheology and processability. However, achieving uniform thickness, surface coverage, and crystallinity over large areas remains a technical challenge. Defects or pinholes at the ETL level can severely impact device performance by inducing shunt pathways and recombination losses [190].

3.7.2 Reproducibility

Reproducibility is another critical challenge in the practical use of ETLs. The consistency of device performance across batches and production runs is essential for commercial reliability and consumer confidence. However, many ETLs especially those involving complex synthesis steps or sensitive precursor chemistries are prone to variation in properties such as thickness, stoichiometry, morphology, and defect density [232]. Even slight inconsistencies in ETL quality can significantly affect charge extraction efficiency, energy level alignment, and interfacial recombination, leading to fluctuating device efficiencies [232]. This issue is particularly prominent with solution-processed or low-temperature ETLs, where environmental factors like humidity, solvent evaporation rate, or precursor aging can introduce variability. To mitigate this, standardization of precursor preparation, automation of coating processes, and in-line quality control measures are being developed in industrial pilot lines. Additionally, the use of robust and stoichiometrically stable materials, such as pre-synthesized SnO_2 nanoparticles, offers a pathway to more consistent film properties [233, 234].

3.7.3 Long-term stability in practical ETL integration

Perhaps the most pressing concern for commercial ETL integration is long-term stability under operational conditions.

In a practical solar module, the ETL must endure prolonged exposure to sunlight (UV irradiation), heat, moisture, and electrical bias conditions under which many lab-scale devices deteriorate [235]. Some ETL materials, particularly ZnO, are known to catalyze the degradation of the adjacent perovskite layer, especially in the presence of moisture or acidic decomposition products. This degradation arises from chemical incompatibilities at the ETL/perovskite interface, which can trigger the breakdown of the perovskite structure or lead to ion migration and trap formation. Moreover, some low-temperature ETLs may contain residual organics or precursors that destabilize the perovskite or lead to unwanted interface reactions. As a result, interface engineering including passivation layers, self-assembled monolayers, or buffer interlayers is increasingly used to suppress chemical reactions and improve device durability [236, 237]. Thermal stability is another key aspect of long-term ETL reliability. During outdoor operation, solar cells can reach temperatures above 60 °C. The ETL must maintain its structural and electronic integrity without undergoing phase transitions, film cracking, or delamination [238]. Inorganic materials generally outperform organic ETLs in this regard, but even within inorganics, material selection and processing conditions significantly influence thermal robustness. Encapsulation can mitigate some degradation, but it adds to manufacturing complexity and cost, underscoring the need for inherently stable ETL materials [239].

Achieving successful integration of ETLs into scalable, reproducible, and stable perovskite solar modules is a multifaceted challenge. It demands not only materials with excellent intrinsic electronic properties but also compatibility with industrial processing, environmental resilience, and reproducibility across large batches. Moving forward, research must focus not only on new ETL materials but also on process engineering, interface design, and system-level optimization to bridge the gap between laboratory prototypes and commercial photovoltaic products. Only by addressing these practical constraints can ETLs unlock their full potential in accelerating the commercialization of perovskite solar technologies.

3.8 SnO_2: the superior electron transport layer for perovskite solar cells

SnO_2 has emerged as the superior ETL in PSCs, surpassing traditional materials like TiO_2 and ZnO. One of the primary reasons for its superiority is its exceptional electron mobility, which facilitates faster and more efficient charge transport. Unlike TiO_2, which suffers from relatively low electron mobility and higher trap densities, SnO_2 enables rapid charge extraction, minimizing recombination losses and enhancing overall device efficiency [149]. This characteristic is crucial in PSCs, where efficient electron transport directly influences PCE and operational stability. In addition to its high electron mobility, SnO_2 offers a more favorable conduction band alignment with perovskite materials, reducing the energy barrier for electron transfer. This optimized energy-level alignment ensures better charge extraction while suppressing charge accumulation at the interface, which can otherwise lead to recombination losses and device degradation [37]. Furthermore, SnO_2 exhibits excellent optical transparency, allowing maximum light absorption in the perovskite layer and contributing to higher photocurrent generation. Another key advantage of SnO_2 over other ETLs is its superior chemical stability. TiO_2, for instance, is known to undergo photocatalytic degradation under UV exposure, leading to instability in PSCs over time. In contrast, SnO_2 remains stable under UV illumination and harsh environmental conditions, making it an ideal choice for long-term device performance. Additionally, SnO_2 can be processed at low temperatures, making it compatible with flexible and large-scale manufacturing, a significant advantage for commercial applications [42].

Moreover, advancements in interface engineering and surface modification techniques have further solidified SnO_2 position as the leading ETL [240]. Surface passivation strategies effectively reduce defect states at the SnO_2/perovskite interface, mitigating non-radiative recombination losses. Doping and nanostructuring techniques have also been explored to optimize SnO_2 electrical properties, further improving the efficiency and stability of PSCs. These collective attributes make SnO_2 the most promising ETL for next-generation perovskite solar cells, offering a balance of high efficiency, stability, and scalability.

4 Conclusion

In this review, we have demonstrated the pivotal role of inorganic ETLs in advancing the efficiency and stability of PSCs. We explore the properties, morphologies, preparation methods, and optimization strategies of various ETLs for PSCs. Each ETL presents unique advantages and limitations. TiO_2 offers excellent chemical stability and charge transport but suffers from high-temperature processing and UV-induced degradation. ZnO boasts high electron mobility and low temperature processability but faces severe interface recombination and instability. SnO_2, with its favorable energy band alignment, high electron mobility, low-temperature synthesis, and weak photocatalysis, emerges as a promising candidate, though it still faces challenges like surface defects and interface recombination. Despite significant progress, no single ETL fully meets the requirements of efficiency, stability, and scalability. Therefore, ongoing

research focuses on optimizing ETLs to enhance energy alignment, crystal structure, electron transport, and film morphology while minimizing defects. Achieving higher efficiency and stability in PSCs remains a key challenge, as inherent defects in ETLs impact performance and induce hysteresis. Numerous ETLs with promising stability and nanostructures have been developed alongside optimization strategies to enhance device performance. However, commercialization demands scalable, cost-effective, and high-quality ETLs that are dense, uniform, and defect-free. Additionally, low-temperature fabrication is crucial for reducing costs, minimizing energy consumption, and enabling flexible devices. Continued research in ETL development and device physics is essential to advancing high-performance PSCs toward commercial viability.

5 Future prospect

Future research should focus on discovering and synthesizing new inorganic materials that can outperform current ETLs like TiO_2, ZnO, and SnO_2. This includes exploring novel compounds with enhanced electron mobility and stability under operational conditions. The integration of advanced materials could lead to significant improvements in PCEs of PSCs. A critical area for future work is the optimization of interface engineering techniques. By minimizing defects and reducing recombination rates at the ETL surface, researchers can enhance charge transport dynamics. This will be essential for maximizing the efficiency and longevity of PSCs. As the demand for renewable energy sources grows, the scalability and cost-effectiveness of ETL materials will be paramount. Future studies should prioritize the development of ETLs that can be produced at scale without compromising performance. This includes investigating low-temperature processing methods that can facilitate mass production. The future of inorganic ETLs may also involve their integration with emerging technologies such as tandem solar cells and flexible photovoltaics. This could open new avenues for enhancing the overall efficiency and application range of PSCs, making them more versatile in various environments. Addressing the long-term stability of ETLs under real-world conditions is crucial. Future research should focus on understanding the degradation mechanisms of ETLs and developing strategies to mitigate these issues, ensuring that PSCs maintain high performance over extended periods. Continued exploration of doping strategies and surface modifications will be vital for optimizing the performance of inorganic ETLs. These techniques can significantly influence charge transport properties and device efficiency, making them a key area for future investigation.

Acknowledgements Abubakar Sadiq Yusuf would like to thank the Tertiary Education Trust Fund (Tetfund) for funding TETF/ES/UNIV/NIGER STATE/TSAS/2020. This project was partly funded by the Royal Society of New Zealand under Marsden contract MFP-GNS2202 and by the New Zealand Ministry for Business, Innovation and Employment through the Materials for Low Carbon Future Program (C05X1702).

Author contributions **Abubakar Sadiq Yusuf**: Conceptualization, Writing - original draft, Writing - review & editing, Resources. **Martin Markwitz**: Visualization, Writing - review & editing. **Holger Fiedler**: Visualization, Supervision, Funding Acquisition, Writing - review & editing. **Zhan Chen**: Supervision, Writing - review & editing. **Maziar Ramezani**: Supervision, Writing - review & editing. **John V. Kennedy**: Supervision, Funding Acquisition, Writing - review & editing.

Funding Open Access funding enabled and organized by CAUL and its Member Institutions

Data availability No data was used.

Declarations

Competing interest The authors assert that they own no identifiable conflicting financial interests or personal affiliations that may have impacted the work presented in this research.

References

1. A. Sharif et al., Exploring the impact of green technology, renewable energy and globalization towards environmental sustainability in the top ecological impacted countries. Geosci. Front. **15**(6), 101895 (2024). https://doi.org/10.1016/j.gsf.2024.101895
2. N. Kannan, D. Vakeesan, Solar energy for future world: - a review. Renew. Sustain. Energy Rev. **62**, 1092–1105 (2016). https://doi.org/10.1016/j.rser.2016.05.022
3. J.Y. Kim et al., High-efficiency perovskite solar cells. Chem. Rev. **120**(15), 7867–7918 (2020). https://doi.org/10.1021/acs.chemrev.0c00107
4. M. Liu, M.B. Johnston, H.J. Snaith, Efficient planar heterojunction perovskite solar cells by vapour deposition. Nature **501**(7467), 395–398 (2013). https://doi.org/10.1038/nature12509
5. H.-S. Kim et al., Lead iodide perovskite sensitized all-solid-state submicron thin film mesoscopic solar cell with efficiency exceeding 9%. Sci. Rep. **2**(1), 591 (2012). https://doi.org/10.1038/srep00591

6. A. Kojima et al., Organometal halide perovskites as visible-light sensitizers for photovoltaic cells. J. Am. Chem. Soc. **131**(17), 6050–6051 (2009). https://doi.org/10.1021/ja809598r
7. Y. Huang et al., *High-Efficiency Inverted Perovskite Solar Cells via In Situ Passivation Directed Crystallization.* Advanced Materials, 2024. 36(41): p. 2408101 https://doi.org/10.1002/adma.202408101
8. E.H. Anaraki et al., Highly efficient and stable planar perovskite solar cells by solution-processed tin oxide. Energy Environ. Sci. **9**(10), 3128–3134 (2016). https://doi.org/10.1039/C6EE02390H
9. M. Green et al., Solar cell efficiency tables (version 57). Prog. Photovoltaics Res. Appl. **29**(1), 3–15 (2020). https://doi.org/10.1002/pip.3371
10. M. Grätzel, Dye-sensitized solid-state heterojunction solar cells. MRS Bull. **30**(1), 23–27 (2005)
11. S. Yun et al., New-generation integrated devices based on dye-sensitized and perovskite solar cells. Energy Environ. Sci. **11**(3), 476–526 (2018). https://doi.org/10.1039/C7EE03165C
12. U. Bach et al., *Solid-state dye-sensitized mesoporous TiO_2solar cells with high photon-to-electron conversion efficiencies*. Nature **395**(6702), 583–585 (1998). https://doi.org/10.1038/26936
13. J. Cameron, P.J. Skabara, Organic electron transport materials. Beilstein J. Org. Chem. **20**, 672–674 (2024). https://doi.org/10.3762/bjoc.20.60
14. A.A. Said, J. Xie, Q. Zhang, Recent progress in organic electron transport materials in inverted perovskite solar cells. Small **15**(27), 1900854 (2019). https://doi.org/10.1002/smll.201900854
15. W. Zhang et al., Recent advance in solution-processed organic interlayers for high-performance planar perovskite solar cells. Adv. Sci. **5**(7), 1800159 (2018). https://doi.org/10.1002/advs.201800159
16. T. Zhang et al., Recent progress in improving strategies of inorganic electron transport layers for perovskite solar cells. Nano Energy **104**, 107918 (2022). https://doi.org/10.1016/j.nanoen.2022.107918
17. A.D. Racovita, Titanium dioxide: structure, impact, and toxicity. Int. J. Environ. Res. Public Health (2022). https://doi.org/10.3390/ijerph19095681
18. A.E. Shalan et al., *Retraction note: A facile low temperature synthesis of TiO_2nanorods for high efficiency dye sensitized solar cells*. Appl. Phys. A **131**(8), 634 (2025). https://doi.org/10.1007/s00339-025-08786-3
19. G. Guo, H. Zhang, The effect of morphology of ZnO particle on properties of asphalt binder and mixture. Int. J. Transp. Sci. Technol. **11**(3), 437–454 (2022). https://doi.org/10.1016/j.ijtst.2021.05.005
20. G. Bai et al., *High performance perovskite sub-module with sputtered SnO_2electron transport layer*. Solar Energy **183**, 306–314 (2019). https://doi.org/10.1016/j.solener.2019.03.026
21. F. Ali, S. Gupta, A statistical design of experiments and structural characterization of ITO for perovskite solar cells. Appl. Phys. A **131**(8), 648 (2025). https://doi.org/10.1007/s00339-025-08794-3
22. C. Luo et al., *Perovskite Tandems: the Next Big Leap in Photovoltaic Technology.* Advanced Materials, 2025. n/a(n/a): p. e08331 https://doi.org/10.1002/adma.202508331
23. K.T. Tanko et al., Stability and reliability of perovskite photovoltaics: are we there yet? MRS Bull. **50**(4), 512–525 (2025). https://doi.org/10.1557/s43577-025-00863-5
24. B. Zhang et al., Recent advances in tin halide perovskite solar cells: a critical review. J. Mater. Chem. A (2025). https://doi.org/10.1039/D5TA04568A
25. M. Bissenova et al., Hybrid adsorption–photocatalysis composites: a sustainable route for efficient water purification. Mater. Renew. Sustain. Energy **14**(2), 44 (2025). https://doi.org/10.1007/s40243-025-00319-5
26. D. Wang et al., Photocatalysis assisted solar-driven interfacial water evaporation: principles, advances and trends. Sep. Purif. Technol. **360**, 130975 (2025). https://doi.org/10.1016/j.seppur.2024.130975
27. V.E. Madhavan et al., Copper thiocyanate inorganic hole-transporting material for high-efficiency perovskite solar cells. ACS Energy Lett. **1**(6), 1112–1117 (2016). https://doi.org/10.1021/acsenergylett.6b00501
28. C.W. Myung, G. Lee, K.S. Kim, *La-doped $BaSnO_3$electron transport layer for perovskite solar cells*. J. Mater. Chem. A **6**(45), 23071–23077 (2018). https://doi.org/10.1039/C8TA08764D
29. M. Zhu et al., Graphene-modified tin dioxide for efficient planar perovskite solar cells with enhanced electron extraction and reduced hysteresis. ACS Appl. Mater. Interfaces **11**(1), 666–673 (2019). https://doi.org/10.1021/acsami.8b15665
30. J. Han et al., Interfacial engineering of a ZnO electron transporting layer using self-assembled monolayers for high performance and stable perovskite solar cells. J. Mater. Chem. A **8**(4), 2105–2113 (2020). https://doi.org/10.1039/C9TA12750J
31. Y. Sun et al., *In situ* ligand-managed SnO_2 electron transport layer for high-efficiency and stable perovskite solar cells. Adv. Funct. Mater. **34**(51), 2410165 (2024). https://doi.org/10.1002/adfm.202410165
32. G. Yang et al., *Effective carrier-concentration tuning of SnO_2quantum dot electron-selective layers for high-performance planar perovskite solar cells*. Adv. Mater. **30**(14), 1706023 (2018). https://doi.org/10.1002/adma.201706023
33. K. Xiao et al., Solution-processed monolithic all-perovskite triple-junction solar cells with efficiency exceeding 20%. ACS Energy Lett. **5**(9), 2819–2826 (2020). https://doi.org/10.1021/acsenergylett.0c01184
34. Y. Zhao et al., *Thick TiO_2-based top electron transport layer on perovskite for highly efficient and stable solar cells*. ACS Energy Lett. **3**(12), 2891–2898 (2018). https://doi.org/10.1021/acsenergylett.8b01507
35. H. Niu et al., Magnetron sputtered ZnO electron transporting layers for high performance perovskite solar cells. Dalton Trans. **50**(19), 6477–6487 (2021). https://doi.org/10.1039/D1DT00344E
36. A. Uddin, H. Yi, *Progress and challenges of SnO_2* electron transport layer for perovskite solar cells: a critical review. Solar RRL (2022). https://doi.org/10.1002/solr.202100983
37. Q. Jiang, X. Zhang, J. You, *SnO_2: A wonderful electron transport layer for perovskite solar cells*. Small **14**(31), 1801154 (2018). https://doi.org/10.1002/smll.201801154
38. W. Hu et al., *Low-Temperature In Situ Amino Functionalization of TiO_2Nanoparticles Sharpens Electron Management Achieving over 21% Efficient Planar Perovskite Solar Cells*. Adv. Mater. **31**(8), 1806095 (2019). https://doi.org/10.1002/adma.201806095
39. G. Yang et al., Recent progress in electron transport layers for efficient perovskite solar cells. J. Mater. Chem. A **4**(11), 3970–3990 (2016). https://doi.org/10.1039/c5ta09011c
40. A.K. Jena, A. Kulkarni, T. Miyasaka, Halide perovskite photovoltaics: background, status, and future prospects. Chem. Rev. **119**(5), 3036–3103 (2019). https://doi.org/10.1021/acs.chemrev.8b00539
41. Q. Dong et al., *Improved SnO_2electron transport layers solution-deposited at near room temperature for rigid or flexible perovskite solar cells with high efficiencies*. Adv. Energy Mater. **9**(26), 1900834 (2019). https://doi.org/10.1002/aenm.201900834
42. Q. Dong et al., *Energetically favored formation of SnO_2nanocrystals as electron transfer layer in perovskite solar cells with high efficiency exceeding 19%*. Nano Energy **40**, 336–344 (2017). https://doi.org/10.1016/j.nanoen.2017.08.041
43. Y. Chen et al., *SnO_2*-based electron transporting layer materials for perovskite solar cells: a review of recent progress. J. Energy

Chem. **35**, 144–167 (2019). https://doi.org/10.1016/j.jechem.2018.11.011
44. P. Zhang et al., Perovskite solar cells with ZnO electron-transporting materials. Adv. Mater. **30**(3), 1703737 (2018). https://doi.org/10.1002/adma.201703737
45. R. Keshtmand, M.R. Zamani-Meymian, N. Taghavinia, *Improving the performance of planar perovskite solar cell using NH_4Cl treatment of SnO_2as electron transport layer*. Surf. Interfaces **28**, 101596 (2022). https://doi.org/10.1016/j.surfin.2021.101596
46. A. Kumar et al., Enhanced efficiency and stability of electron transport layer in perovskite tandem solar cells: challenges and future perspectives. Solar Energy **266**, 112185 (2023). https://doi.org/10.1016/j.solener.2023.112185
47. J.-X. Song et al., Low-temperature-processed metal oxide electron transport layers for efficient planar perovskite solar cells. Rare Met. **40**(10), 2730–2746 (2021). https://doi.org/10.1007/s12598-020-01676-y
48. H. Soliman, A.S.H. Makhlouf, D. Rayan, Dual-function film of ZnO doped into CrNi black coatings as solar absorbent and corrosion resistant. Appl. Phys. A **130**(12), 923 (2024). https://doi.org/10.1007/s00339-024-07961-2
49. S. Ali et al., Simulation of lead-free perovskite solar cells with improved performance. Crystals (2025). https://doi.org/10.3390/cryst15020171
50. K.K. Sharma et al., *(111) facet-engineered Sno_2* as an electron transport layer for efficient and stable triple-cation perovskite solar cells. Sustain. Energy Fuels **9**(11), 3102–3109 (2025). https://doi.org/10.1039/D5SE00339C
51. M.S. Reza et al., *A* comprehensive investigation involving numerous HTL and ETL layers to design and simulate high-efficiency *Ca_3AsI_3*-based perovskite solar cells. Inorg. Chem. Commun. **172**, 113647 (2025). https://doi.org/10.1016/j.inoche.2024.113647
52. F.L. Rahim et al., *Computational study of highly efficient SnO_2 ETL-based inorganic perovskite solar cell*. Przegląd Elektrotechniczny, 2024. 2024(11).
53. A. Basit, I. Qasim, *Optimizing solar cell and module design with SnO_2-ETL and organometal-halide perovskite absorber: SCAPS-1D and PVSyst analysis*. Wirel. Power Transf. (2025). https://doi.org/10.48130/wpt-0024-0015
54. M. Meskini, S. Asgharizadeh, *Performance simulation of the perovskite solar cells with Ti_3C_2MXene in the SnO_2electron transport layer*. Sci. Rep. **14**(1), 5723 (2024). https://doi.org/10.1038/s41598-024-56461-z
55. H. Li et al., Photoferroelectric perovskite solar cells: principles, advances and insights. Nano Today **37**, 101062 (2021). https://doi.org/10.1016/j.nantod.2020.101062
56. M.K. Hossain et al., *An* extensive study on multiple ETL and HTL layers to design and simulation of high-performance lead-free $CsSnCl_3$-based perovskite solar cells. Sci. Rep. **13**(1), 2521 (2023). https://doi.org/10.1038/s41598-023-28506-2
57. N.K. Elangovan et al., Recent developments in perovskite materials, fabrication techniques, band gap engineering, and the stability of perovskite solar cells. Energy Rep. **11**, 1171–1190 (2024). https://doi.org/10.1016/j.egyr.2023.12.068
58. T. Xue et al., *Preparation of TiO_2/SnO_2* electron transport layer for performance enhancement of all-inorganic perovskite solar cells using electron beam evaporation at low temperature. Micromachines (2023). https://doi.org/10.3390/mi14081549
59. V.S. Katta et al., *Deciphering the role of Er^{3+}/Nd^{3+}co-doping effect on TiO_2as an improved electron transport layer in perovskite solar cells*. Solar Energy **262**, 111801 (2023). https://doi.org/10.1016/j.solener.2023.111801
60. L. Chih-Wei et al., *UV degradation mechanism of TiO_2-based perovskite solar cells studied by pump-probe spectroscopy*. in *Proc.SPIE*. 2020. https://doi.org/10.1117/12.2554174
61. G.G. Njema, J.K. Kibet, A review of chalcogenide-based perovskites as the next novel materials: solar cell and optoelectronic applications, catalysis and future perspectives. Next Nanotechnol **7**, 100102 (2025). https://doi.org/10.1016/j.nxnano.2024.100102
62. M. Stramarkou et al., *Fabrication of ZnO thin films doped with Na at different percentages for sensing CO_2* in small quantities at room temperature. Sensors **25**(9), 2705 (2025). https://doi.org/10.3390/s25092705
63. Y. Taneja, D. Dube, R. Singh, Recent advances in elemental doping and simulation techniques: improving structural, photophysical and electronic properties of titanium dioxide. J. Mater. Chem. C **12**(37), 14774–14808 (2024). https://doi.org/10.1039/D4TC02031F
64. L.K. Tinoco Navarro, C. Jaroslav, *Enhancing photocatalytic properties of TiO_2 Photocatalyst and heterojunctions: A comprehensive review of the impact of biphasic systems in aerogels and xerogels Synthesis, Methods, and mechanisms for environmental applications*. Gels. **9**(12) (2023). https://doi.org/10.3390/gels9120976
65. M.-M. Huo et al., Morphology and carrier non-geminate recombination dynamics regulated by solvent additive in polymer/fullerene solar cells. RSC Adv. **10**(39), 23128–23135 (2020). https://doi.org/10.1039/D0RA03389H
66. Y. Zhang, R. Dai, S. Hu, *Study of the role of oxygen vacancies as active sites in reduced graphene oxide-modified TiO_2*. Phys. Chem. Chem. Phys. **19**(10), 7307–7315 (2017). https://doi.org/10.1039/C7CP00630F
67. X. Wang et al., Cerium oxide standing out as an electron transport layer for efficient and stable perovskite solar cells processed at low temperature. J. Mater. Chem. A **5**(4), 1706–1712 (2017). https://doi.org/10.1039/C6TA07541J
68. A.S. Yusuf et al., Effect of electron transport Layers, interface defect density and working temperature on perovskite solar cells using SCAPS 1-D software. East. Eur. J. Phys., **2024**(1): pp. 332–341 https://doi.org/10.26565/2312-4334-2024-1-31
69. A.S. Yusuf et al., A review of coating tin oxide electron transport layer for optimizing the performance of perovskite solar cells. Chemistry of Inorganic Materials **6**, 100100 (2025). https://doi.org/10.1016/j.cinorg.2025.100100
70. M. Shekargoftar et al., *Low-temperature and rapid deposition of an SnO_2layer from a colloidal nanoparticle dispersion for use in planar perovskite solar cells*. Energy Technol. **9**(5), 2001076 (2021). https://doi.org/10.1002/ente.202001076
71. A. Beltrán et al., *Thermodynamic* argument about SnO_2 nanoribbon growth. Appl. Phys. Lett. **83**(4), 635–637 (2003). https://doi.org/10.1063/1.1594837
72. Z. Li, P. Graziosi, N. Neophytou, *Electron and hole mobility of $SnO_2$from Full-Band Electron–Phonon and ionized impurity scattering computations*. Crystals (2022). https://doi.org/10.3390/cryst12111591
73. M.K. Hossain et al., Effect of various electron and hole transport layers on the performance of *CsPbI3*-based perovskite solar cells: a numerical investigation in DFT, SCAPS-1D, and WxAMPS frameworks. ACS Omega **7**(47), 43210–43230 (2022). https://doi.org/10.1021/acsomega.2c05912
74. M. Simenas et al., Phase transitions and dynamics in mixed three- and low-dimensional lead halide perovskites. Chem. Rev. **124**(5), 2281–2326 (2024). https://doi.org/10.1021/acs.chemrev.3c00532
75. M.K. Hossain et al., *A* comprehensive study of the optimization and comparison of cesium halide perovskite solar cells using ZnO and Cu_2FeSnS_4 as charge transport layers. New J. Chem. **47**(18), 8602–8624 (2023). https://doi.org/10.1039/D3NJ00320E
76. M.K. Rabchinskii et al., Rationalizing graphene–ZnO composites for gas sensing via functionalization with amines. Nanomaterials (2024). https://doi.org/10.3390/nano14090735

77. S. Yasmeen et al., *Superior* photodegradation of Bentazon and nile blue and their binary mixture using Sol–Gel synthesized TiO_2 nanoparticles under UV and sunlight sources. Appl. Sci. (2025). https://doi.org/10.3390/app15041899
78. D.R. Eddy et al., *Heterophase polymorph of TiO_2 (Anatase, Rutile, Brookite, TiO_2B for efficient photocatalyst: fabrication and activity*. Nanomaterials (Basel). **13**(4) (2023). https://doi.org/10.3390/nano13040704
79. R. Ponte, E. Rauwel, P. Rauwel, *Tailoring SnO_2defect states and structure: reviewing bottom-up approaches to control size, morphology, electronic and electrochemical properties for application in batteries*. Materials **16**(12), 4339 (2023). https://doi.org/10.3390/ma16124339
80. H.E. Sánchez-Godoy et al., Situ ethanolamine ZnO nanoparticle passivation for perovskite interface stability and highly efficient solar cells. Nanomaterials (Basel). **12**(5) (2022). https://doi.org/10.3390/nano12050823
81. G. Liu et al., Highly efficient and stable ZnO-based MA-free perovskite solar cells via overcoming interfacial mismatch and deprotonation reaction. Chem. Eng. J. **431**, 134235 (2022). https://doi.org/10.1016/j.cej.2021.134235
82. M. Haghighi et al., Low-temperature processing methods for tin oxide as electron transporting layer in scalable perovskite solar cells. Solar RRL **7**(10), 2201080 (2023). https://doi.org/10.1002/solr.202201080
83. Y. Zhao et al., Comprehensive study of Sol–Gel versus Hydrolysis–Condensation methods to prepare ZnO films: electron transport layers in perovskite solar cells. ACS Appl. Mater. Interfaces **9**(31), 26234–26241 (2017). https://doi.org/10.1021/acsami.7b04833
84. Y. Zhou, X. Li, H. Lin, To be higher and stronger—metal oxide electron transport materials for perovskite solar cells. Small **16**(15), 1902579 (2020). https://doi.org/10.1002/smll.201902579
85. T.-Y. Lee et al., Advances in core technologies for semiconductor manufacturing: applications and challenges of atomic layer etching, neutral beam etching and atomic layer deposition. Nanoscale Adv. **7**(10), 2796–2817 (2025). https://doi.org/10.1039/D4NA00784K
86. H. Lu et al., Identifying the optimum thickness of electron transport layers for highly efficient perovskite planar solar cells. J. Mater. Chem. A **3**(32), 16445–16452 (2015). https://doi.org/10.1039/C5TA03686K
87. X. Dong et al., *The* effect of ALD-Zno layers on the formation of $CH_3NH_3PbI_3$ with different perovskite precursors and sintering temperatures. Chem. Commun. **50**(92), 14405–14408 (2014). https://doi.org/10.1039/C4CC04685D
88. Y. Lee et al., Efficient planar perovskite solar cells using passivated tin oxide as an electron transport layer. Adv. Sci. **5**(6), 1800130 (2018). https://doi.org/10.1002/advs.201800130
89. R.C. Ruiz-Ortega et al., Comprehensive analysis of CDS ultrathin films modified by the substrate position inside the reactor container using the CBD technique. ACS Omega **8**(35), 31725–31737 (2023). https://doi.org/10.1021/acsomega.3c02158
90. K. Sun et al., *Over 9% Efficient Kesterite Cu_2ZnSnS_4Solar Cell Fabricated by Using Zn1–xCdxS Buffer Layer*. Adv. Energy Mater. **6**(12), 1600046 (2016). https://doi.org/10.1002/aenm.201600046
91. M.H. Kumar et al., Flexible, low-temperature, solution processed ZnO-based perovskite solid state solar cells. Chem. Commun. **49**(94), 11089–11091 (2013). https://doi.org/10.1039/C3CC46534A
92. J.-Y. Chen et al., *Low-temperature electrodeposited crystalline SnO_2as an efficient electron-transporting layer for conventional perovskite solar cells*. Sol. Energy Mater. Sol. Cells **164**, 47–55 (2017). https://doi.org/10.1016/j.solmat.2017.02.008
93. J. Ma et al., *Highly efficient and stable planar perovskite solar cells with large-scale manufacture of E-beam evaporated SnO_2toward commercialization*. Solar RRL **1**(10), 1700118 (2017). https://doi.org/10.1002/solr.201700118
94. S.H. Im, A.J. Olasoji, *Perspective Chapter: TiO_2 Electron Transporting Layers for Perovskite Solar Cells*, in *Titanium Dioxide - Uses, Applications, and Advances*, ed. by C. Montalvo Romero, C.A. Aguilar, E. Moctezuma (IntechOpen: Rijeka, Editors, 2024)
95. R. Banoth et al., *Surface engineering of mesoporous-TiO_2electron transport layer for improved performance of organic-inorganic perovskite solar cells via suppressing interface defects, enhancing charge extraction and boosting carrier transport*. Colloids Surf A Physicochem. Eng. Aspects **676**, 132075 (2023). https://doi.org/10.1016/j.colsurfa.2023.132075
96. S. Reghunath, D. Pinheiro, S.D. Kr, *A review of hierarchical nanostructures of TiO_2: advances and applications*. Appl. Surf. Sci. Adv. **3**, 100063 (2021). https://doi.org/10.1016/j.apsadv.2021.100063
97. X. Wang et al., *Electron Transport and Recombination in Photoanode of Electrospun TiO_2Nanotubes for Dye-Sensitized Solar Cells*. J. Phys. Chem. C **117**(4), 1641–1646 (2013). https://doi.org/10.1021/jp311725g
98. B. Yang et al., *Low temperature synthesis of hierarchical TiO_2nanostructures for high performance perovskite solar cells by pulsed laser deposition*. Phys. Chem. Chem. Phys. **18**(39), 27067–27072 (2016). https://doi.org/10.1039/C6CP02896A
99. W.Q. Wu et al., *Low-temperature solution-processed amorphous titania nanowire thin films for 1 cm^2perovskite solar cells*. ACS Appl. Mater. Interfaces **12**(10), 11450–11458 (2020). https://doi.org/10.1021/acsami.9b19041
100. W.-J. Lee, M. Alhoshan, W.H. Smyrl, Titanium dioxide nanotube arrays fabricated by anodizing processes: electrochemical properties. J. Electrochem. Soc. **153**(11), B499 (2006). https://doi.org/10.1149/1.2347098
101. S.A. Bakar, C. Ribeiro, Nitrogen-doped titanium dioxide: an overview of material design and dimensionality effect over modern applications. J. Photochem. Photobiol., C **27**, 1–29 (2016). https://doi.org/10.1016/j.jphotochemrev.2016.05.001
102. H. Tan et al., Efficient and stable solution-processed planar perovskite solar cells via contact passivation. Science **355**(6326), 722–726 (2017). https://doi.org/10.1126/science.aai9081
103. H.-S. Kim, N.-G. Park, *Correction to Parameters Affecting I–V Hysteresis of $CH_3NH_3PbI_3$ Perovskite Solar Cells: Effects of Perovskite Crystal Size and Mesoporous TiO_2 Layer*. J. Phys. Chem. Lett. **5**(19), 3434–3434 (2014). https://doi.org/10.1021/jz502009r
104. J. Xu et al., *ZnO-Assisted Growth of $CH_3NH_3PbI_3$–xClx Film and Efficient Planar Perovskite Solar Cells with a TiO_2/ZnO/C60 Electron Transport Trilayer*. ACS Appl. Mater. Interfaces **10**(24), 20578–20590 (2018). https://doi.org/10.1021/acsami.8b05560
105. H. Zhang et al., Roll to roll compatible fabrication of inverted organic solar cells with a self-organized charge selective cathode interfacial layer. J. Mater. Chem. A **4**(14), 5032–5038 (2016). https://doi.org/10.1039/C6TA00391E
106. S.K. Pathak et al., *Performance and Stability Enhancement of Dye-Sensitized and Perovskite Solar Cells by Al Doping of TiO_2*. Adv. Funct. Mater. **24**(38), 6046–6055 (2014). https://doi.org/10.1002/adfm.201401658
107. G. Yin et al., *Enhancing efficiency and stability of perovskite solar cells through Nb-doping of TiO_2at low temperature*. ACS Appl. Mater. Interfaces **9**(12), 10752–10758 (2017). https://doi.org/10.1021/acsami.7b01063
108. M. Zhang et al., *Ti^{3+}self-doping of TiO_2* boosts its photocatalytic performance: a synergistic mechanism. Molecules (2024). https://doi.org/10.3390/molecules29225385

109. J. You et al., Low-temperature solution-processed perovskite solar cells with high efficiency and flexibility. ACS Nano **8**(2), 1674–1680 (2014). https://doi.org/10.1021/nn406020d
110. A. Katoch et al., *Preparation of highly stable TiO_2sols and nanocrystalline TiO_2films via a low temperature sol–gel route*. J. Sol-Gel Sci. Technol. **61**(1), 77–82 (2012). https://doi.org/10.1007/s10971-011-2593-6
111. H. Xie et al., *Low temperature solution-derived TiO_2-SnO_2bilayered electron transport layer for high performance perovskite solar cells*. Appl. Surf. Sci. **464**, 700–707 (2019). https://doi.org/10.1016/j.apsusc.2018.09.146
112. V.P. Hoang Huy, Bark *Review on surface modification of SnO_2 Electron transport layer for High-Efficiency perovskite solar cells*. Appl. Sci. **13** (2023). https://doi.org/10.3390/app131910715
113. Y. Kuang et al., *Low-Temperature Plasma-Assisted Atomic-Layer-Deposited SnO_2as an Electron Transport Layer in Planar Perovskite Solar Cells*. ACS Appl. Mater. Interfaces **10**(36), 30367–30378 (2018). https://doi.org/10.1021/acsami.8b09515
114. V. Rohnacher et al., Analytical study of solution-processed tin oxide as electron transport layer in printed perovskite solar cells. Adv. Mater. Technol. **6**(2), 2000282 (2021). https://doi.org/10.1002/admt.202000282
115. H. Ren et al., *Facile solution Spin-Coating SnO_2thin film covering cracks of TiO_2* hole blocking layer for perovskite solar cells. Coatings (2018). https://doi.org/10.3390/coatings8090314
116. W. Ke et al., Efficient hole-blocking layer-free planar halide perovskite thin-film solar cells. Nat. Commun. **6**(1), 6700 (2015). https://doi.org/10.1038/ncomms7700
117. L. Lin et al., Inorganic electron transport materials in perovskite solar cells. Adv. Funct. Mater. **31**(5), 2008300 (2021). https://doi.org/10.1002/adfm.202008300
118. F. Yu, W. Zhao, S.F. Liu, *A straightforward chemical approach for excellent In_2S_3electron transport layer for high-efficiency perovskite solar cells*. RSC Adv. **9**(2), 884–890 (2019)
119. S. Vijayaraghavan et al., *Low-temperature* processed highly efficient hole transport layer free carbon-based planar perovskite solar cells with SnO_2 quantum dot electron transport layer. Mater. Today Phys. **13**, 100204 (2020)
120. M.I. Ahmed, A. Habib, S.S. Javaid, *Perovskite Solar Cells: Potentials, Challenges, and Opportunities.* International Journal of Photoenergy, 2015. 2015: pp. 1–13 https://doi.org/10.1155/2015/592308
121. W. Ke et al., Efficient hole-blocking layer-free planar halide perovskite thin-film solar cells. Nat. Commun. **6**, 6700 (2015). https://doi.org/10.1038/ncomms7700
122. P. Gupta, V. Rathore, *A comprehensive review: Sno$_2$for photovoltaic and gas sensor applications*. Appl. Innovative Res. (AIR) **1**(3–4), 184–193 (2020)
123. Y. Bai et al., *Facilitating the formation of SnO_2film via hydroxyl groups for efficient perovskite solar cells*. Appl. Surf. Sci. **552**, 149459 (2021). https://doi.org/10.1016/j.apsusc.2021.149459
124. Q. Jiang et al., *Enhanced electron extraction using $SnO_2$for high-efficiency planar-structure $HC(NH_2)_2PbI_3$-based perovskite solar cells*. Nat. Energy **2**(1), 16177 (2016). https://doi.org/10.1038/nenergy.2016.177
125. J.P.C. Baena et al., Highly efficient planar perovskite solar cells through band alignment engineering. Energy Environ. Sci. **8**(10), 2928–2934 (2015)
126. M.S. Kiani et al., *Solution-Processed SnO_2Quantum Dots for the electron transport layer of flexible and printed perovskite solar cells*. Nanomaterials **12**(15), 2615 (2022). https://doi.org/10.3390/nano12152615
127. K.A. Bush et al., 23.6%-efficient monolithic perovskite/silicon tandem solar cells with improved stability. Nat. Energy. **2**(4), 1–7 (2017). https://doi.org/10.1038/nenergy.2017.9
128. L.A. Zafoschnig, *SnOx electron selective layers for perovskite/silicon tandem solar cells using atomic layer deposition*. 2018
129. S. Jeong et al., *Atomic layer deposition of a SnO_2electron-transporting layer for planar perovskite solar cells with a power conversion efficiency of 18.3*. Chem. Commun. **55**(17), 2433–2436 (2019). https://doi.org/10.1039/c8cc09557d
130. E. Köhnen et al., Highly efficient monolithic perovskite silicon tandem solar cells: analyzing the influence of current mismatch on device performance. Sustain. Energy Fuels **3**(8), 1995–2005 (2019). https://doi.org/10.1039/C9SE00120D
131. Y. Shao et al., *Origin* and elimination of photocurrent hysteresis by fullerene passivation in $CH_3NH_3PbI_3$ planar heterojunction solar cells. Nat. Commun. **5**(1), 5784 (2014)
132. A.F. Palmstrom, *Next Generation Thin Film Photovoltaics: Study and Application of Surface Modification and Atomic Layer Deposition* (Stanford University, 2017)
133. V.P. Hoang Huy, C.-W. Bark, *Review on surface modification of SnO_2electron transport layer for high-efficiency perovskite solar cells*. Appl. Sci. **13**(19), 10715 (2023)
134. O. Masala, R. Seshadri, Synthesis routes for large volumes of nanoparticles. Annu. Rev. Mater. Res. **34**, 41–81 (2004)
135. V.P. Hoang Huy, T.M.H. Nguyen, C.W. Bark, *Recent advances of doped SnO_2as electron transport layer for High-Performance perovskite solar cells*. Materials (2023). https://doi.org/10.3390/ma16186170
136. B. Roose et al., *Mesoporous SnO_2* electron selective contact enables UV-stable perovskite solar cells. Nano Energy **30**, 517–522 (2016). https://doi.org/10.1016/j.nanoen.2016.10.055
137. W. Zheng, Y. Zhang, J. Tian, Effect of fluorine doping concentration on semiconductive property of tin dioxide. Chalcogenide Lett. **14**(7), 275–281 (2017)
138. Y.-Z. Zheng et al., Iodine-doped ZnO nanopillar arrays for perovskite solar cells with high efficiency up to 18.24%. J. Mater. Chem. A **5**(24), 12416–12425 (2017)
139. M. Batal, G. Nashed, F.H. Jneed, Conductivity and thermoelectric properties of nanostructure tin oxide thin films. J. Assoc. Arab Univ. Basic Appl. Sci. **15**, 15–20 (2014)
140. C. Wang et al., *High-effective SnO_2-based perovskite solar cells by multifunctional molecular additive engineering*. J. Alloys Compd. **886**, 161352 (2021). https://doi.org/10.1016/j.jallcom.2021.161352
141. S. Kim et al., *Effects of potassium treatment on SnO_2electron transport layers for improvements of perovskite solar cells*. Solar Energy **233**, 353–362 (2022). https://doi.org/10.1016/j.solener.2022.01.053
142. H. Bi et al., Selective contact self-assembled molecules for high-performance perovskite solar cells. eScience **5**(2), 100329 (2025). https://doi.org/10.1016/j.esci.2024.100329
143. J. Xie et al., *Enhanced electronic properties of SnO_2via electron transfer from graphene quantum dots for efficient perovskite solar cells*. ACS Nano **11**(9), 9176–9182 (2017). https://doi.org/10.1021/acsnano.7b04070
144. M. Park et al., *Low-temperature solution-processed Li-doped SnO_2as an effective electron transporting layer for high-performance flexible and wearable perovskite solar cells*. Nano Energy **26**, 208–215 (2016). https://doi.org/10.1016/j.nanoen.2016.04.060
145. L. Xiong et al., *Review on the Application of SnO_2in Perovskite Solar Cells*. Adv. Funct. Mater. **28**(35), 1802757 (2018). https://doi.org/10.1002/adfm.201802757
146. W. Yu et al., Carbon-based perovskite solar cells with electron and hole-transporting/-blocking layers. Mater. Futures. **2**(2), 022101 (2023). https://doi.org/10.1088/2752-5724/acbbc2
147. C. Bai et al., *Electrochemical reduction and ion injection of annealing-free $SnO_2$for high performance perovskite solar cells*.

Adv. Energy Mater. **13**(26), 2300491 (2023). https://doi.org/10.1002/aenm.202300491
148. J. Song et al., *Colloidal synthesis of Y-doped SnO_2nanocrystals for efficient and slight hysteresis planar perovskite solar cells*. Solar Energy **185**, 508–515 (2019). https://doi.org/10.1016/j.solener.2019.04.084
149. B. Dahal et al., *Enhancing the performance of the perovskite solar cells by modifying the SnO_2electron transport layer*. J. Phys. Chem. Solids **181**, 111532 (2023). https://doi.org/10.1016/j.jpcs.2023.111532
150. L. Zhu et al., Doping in semiconductor oxides-based electron transport materials for perovskite solar cells application. Solar RRL **5**(3), 2000605 (2021). https://doi.org/10.1002/solr.202000605
151. V.P. Hoang Huy, Bark *Polymer-Doped SnO_2 as an electron transport layer for highly efficient and stable perovskite solar cells*. Polymers. **16** (2024). https://doi.org/10.3390/polym16020199
152. Y. Bai et al., *Low temperature solution-processed Sb:SnO_2nanocrystals for efficient planar perovskite solar cells*. ChemSusChem **9**(18), 2686–2691 (2016). https://doi.org/10.1002/cssc.201600944
153. Z. Xu et al., *La-doped SnO_2as ETL for efficient planar-structure hybrid perovskite solar cells*. Org. Electron. **73**, 62–68 (2019). https://doi.org/10.1016/j.orgel.2019.03.053
154. J. Bahadur et al., *Solution processed Mo doped SnO_2as an effective ETL in the fabrication of low temperature planer perovskite solar cell under ambient conditions*. Org. Electron. **67**, 159–167 (2019). https://doi.org/10.1016/j.orgel.2019.01.027
155. W. Hui et al., *Red-Carbon-Quantum-Dot-Doped SnO_2Composite with Enhanced Electron Mobility for Efficient and Stable Perovskite Solar Cells*. Adv. Mater. **32**(4), 1906374 (2020). https://doi.org/10.1002/adma.201906374
156. E. Halvani Anaraki et al., *Low-Temperature Nb-Doped SnO_2Electron-Selective Contact Yields over 20% Efficiency in Planar Perovskite Solar Cells*. ACS Energy Lett. **3**(4), 773–778 (2018). https://doi.org/10.1021/acsenergylett.8b00055
157. M.S. Kiani et al., *Solution-Processed SnO_2Quantum Dots for the electron transport layer of flexible and printed perovskite solar cells*. Nanomaterials (2022). https://doi.org/10.3390/nano12152615
158. M. Zhong et al., *Highly efficient flexible $MAPbI_3$solar cells with a fullerene derivative-modified SnO_2layer as the electron transport layer*. J. Mater. Chem. A **7**(12), 6659–6664 (2019). https://doi.org/10.1039/C9TA00398C
159. S. Zheng et al., Materials and structures for the electron transport layer of efficient and stable perovskite solar cells. Sci. China Chem. **62**(7), 800–809 (2019). https://doi.org/10.1007/s11426-019-9469-1
160. P. Zhang et al., Perovskite solar cells with ZnO electron-transporting materials. Adv. Mater. **30**(3), 1703737 (2018)
161. C. Zhang et al., Inorganic halide perovskite materials and solar cells. APL Mater. (2019). https://doi.org/10.1063/1.5117306
162. J. You et al., Improved air stability of perovskite solar cells via solution-processed metal oxide transport layers. Nat. Nanotechnol. **11**(1), 75–81 (2016)
163. H. Krysova et al., High-quality dense ZnO thin films: work function and photo/electrochemical properties. J. Solid State Electrochem. **28**(8), 2531–2546 (2024). https://doi.org/10.1007/s10008-023-05766-6
164. Y. Lee et al., Enhanced high-energy proton radiation hardness of ZnO thin-film transistors with a passivation layer. Nano Convergence **12**(1), 7 (2025). https://doi.org/10.1186/s40580-025-00474-5
165. M.A. Mahmud et al., Low temperature processed ZnO thin film as electron transport layer for efficient perovskite solar cells. Sol. Energy Mater. Sol. Cells **159**, 251–264 (2017). https://doi.org/10.1016/j.solmat.2016.09.014
166. L. Xu et al., ZnO with different morphologies synthesized by solvothermal methods for enhanced photocatalytic activity. Chem. Mater. **21**(13), 2875–2885 (2009). https://doi.org/10.1021/cm900608d
167. D. Zheng et al., Combustion synthesized zinc oxide electron-transport layers for efficient and stable perovskite solar cells. Adv. Funct. Mater. **29**(16), 1900265 (2019). https://doi.org/10.1002/adfm.201900265
168. A. Dymshits, L. Iagher, Etgar *Parameters influencing the growth of ZnO nanowires as efficient low temperature flexible Perovskite-Based solar cells*. Materials. **9** (2016). https://doi.org/10.3390/ma9010060
169. C.M. Pelicano, H. Yanagi, Efficient solid-state perovskite solar cells based on nanostructured zinc oxide designed by strategic low temperature water oxidation. J. Mater. Chem. C **5**(32), 8059–8070 (2017). https://doi.org/10.1039/C7TC01934C
170. N.A. Zainal Abidin et al., Dopant engineering for ZnO electron transport layer towards efficient perovskite solar cells. RSC Adv. **13**(48), 33797–33819 (2023). https://doi.org/10.1039/D3RA04823C
171. R. Sha et al., ZnO nano-structured based devices for chemical and optical sensing applications. Sensors Actuators Rep. **4**, 100098 (2022). https://doi.org/10.1016/j.snr.2022.100098
172. A. Janotti, C.G. de Van Walle, Fundamentals of zinc oxide as a semiconductor. Rep. Prog. Phys. **72**(12), 126501 (2009). https://doi.org/10.1088/0034-4885/72/12/126501
173. X. Liu et al., In-doped ZnO electron transport layer for high-efficiency ultrathin flexible organic solar cells. Adv. Sci. **11**(37), e2402158 (2024). https://doi.org/10.1002/advs.202402158
174. Y. Sun et al., Preparations and applications of zinc oxide based photocatalytic materials. Advanced Sensor and Energy Materials **2**(3), 100069 (2023). https://doi.org/10.1016/j.asems.2023.100069
175. H. Mohammadian-Sarcheshmeh, M. Mazloum-Ardakani, Recent advancements in compact layer development for perovskite solar cells. Heliyon **4**(11), e00912 (2018). https://doi.org/10.1016/j.heliyon.2018.e00912
176. J. Zhang et al., *Zno*-PCBM bilayers as electron transport layers in low-temperature processed perovskite solar cells. Sci. Bull. **63**(6), 343–348 (2018). https://doi.org/10.1016/j.scib.2018.02.004
177. Y. Cheng et al., Decomposition of organometal halide perovskite films on zinc oxide nanoparticles. ACS Appl. Mater. Interfaces **7**(36), 19986–19993 (2015). https://doi.org/10.1021/acsami.5b04695
178. R. Azmi et al., High-efficiency air-stable colloidal quantum dot solar cells based on a potassium-doped ZnO electron-accepting layer. ACS Appl. Mater. Interfaces **10**(41), 35244–35249 (2018). https://doi.org/10.1021/acsami.8b12577
179. M. Yue et al., *Optimizing the performance of $CsPbI_3$-based perovskite solar cells via doping a ZnO electron transport layer coupled with interface engineering*. Nano-Micro Lett. **11**(1), 91 (2019). https://doi.org/10.1007/s40820-019-0320-y
180. A. Baktash, O. Amiri, A. Sasani, *Improve efficiency of perovskite solar cells by using Magnesium doped ZnO and TiO_2compact layers*. Superlattices Microstruct. **93**, 128–137 (2016). https://doi.org/10.1016/j.spmi.2016.01.026
181. M.M. Islam, T. Yoshida, Y. Fujita, Effects of ambience on thermal-diffusion type Ga-doping process for ZnO nanoparticles. Coatings (2022). https://doi.org/10.3390/coatings12010057
182. K. Mahmood et al., Indium-doped ZnO mesoporous nanofibers as efficient electron transporting materials for perovskite solar cells. Surf. Coat. Technol. **352**, 231–237 (2018). https://doi.org/10.1016/j.surfcoat.2018.08.039

183. A.E. Shalan et al., Tin-zinc-oxide nanocomposites SZO as promising electron transport layers for efficient and stable perovskite solar cells. Nanoscale Adv. **1**(7), 2654–2662 (2019). https://doi.org/10.1039/c9na00182d
184. R. Azmi et al., High efficiency low-temperature processed perovskite solar cells integrated with alkali metal doped ZnO electron transport layers. ACS Energy Lett. **3**(6), 1241–1246 (2018). https://doi.org/10.1021/acsenergylett.8b00493
185. K. Sekar et al., Control of ZnO nanowires growth in flexible perovskite solar cells: a mini-review. Heliyon **10**(3), e24706 (2024). https://doi.org/10.1016/j.heliyon.2024.e24706
186. L.-C. Chen, Z.-L. Tseng, *ZnO-Based Electron Transporting Layer for Perovskite Solar Cells, in Nanostructured Solar Cells*, ed. by N. Das (IntechOpen: Rijeka, Editor, 2017)
187. S. Sajid et al., Fabricating planar perovskite solar cells through a greener approach. Nanomaterials (2024). https://doi.org/10.3390/nano14070594
188. V. Larini et al., Sustainable and circular management of perovskite solar cells via green recycling of electron transport layer-coated transparent conductive oxide. Adv. Funct. Mater. **34**(50), 2306040 (2024). https://doi.org/10.1002/adfm.202306040
189. H. Luo et al., Bioinspired cage traps for closed-loop lead management of perovskite solar cells under real-world contamination assessment. Nat. Commun. **14**(1), 4730 (2023). https://doi.org/10.1038/s41467-023-40421-8
190. W. Ke et al., Low-temperature solution-processed tin oxide as an alternative electron transporting layer for efficient perovskite solar cells. J. Am. Chem. Soc. **137**(21), 6730–6733 (2015)
191. M. Kim et al., *Conformal quantum dot-SnO_2layers as electron transporters for efficient perovskite solar cells*. Science **375**(6578), 302–306 (2022). https://doi.org/10.1126/science.abh1885
192. M. Kim et al., *Enhanced electrical properties of Li-salts doped mesoporous TiO_2in perovskite solar cells*. Joule **5**(3), 659–672 (2021). https://doi.org/10.1016/j.joule.2021.02.007
193. D. Zheng et al., Combustion synthesized zinc oxide electron-transport layers for efficient and stable perovskite solar cells. Adv. Funct. Mater. **29**(16), 1900265 (2019)
194. H. Guo et al., *Low-temperature processed yttrium-doped $SrSnO_3$perovskite electron transport layer for planar heterojunction perovskite solar cells with high efficiency*. Nano Energy **59**, 1–9 (2019)
195. Y. Hou et al., A band-edge potential gradient heterostructure to enhance electron extraction efficiency of the electron transport layer in high-performance perovskite solar cells. Adv. Funct. Mater. **27**(27), 1700878 (2017)
196. Z. Rao et al., *Revisit of amorphous semiconductor $InGaZnO_4$*: a new electron transport material for perovskite solar cells. J. Alloys Compd. **789**, 276–281 (2019)
197. J. Wei et al., *UV-inert $ZnTiO_3$electron selective layer for photostable perovskite solar cells*. Adv. Energy Mater. **9**(40), 1901620 (2019)
198. E. Zhao et al., *In situ fabrication of 2D SnS_2 nanosheets as a new electron transport layer for perovskite solar cells*. Nano Res. **11**, 5913–5923 (2018)
199. F. Xie et al., *TiO_2-B as an electron transporting material for highly efficient perovskite solar cells*. J. Power Sources **415**, 8–14 (2019). https://doi.org/10.1016/j.jpowsour.2019.01.041
200. S. Wang et al., Water-soluble triazolium ionic-liquid-induced surface self-assembly to enhance the stability and efficiency of perovskite solar cells. Adv. Funct. Mater. **29**(15), 1900417 (2019). https://doi.org/10.1002/adfm.201900417
201. M. Kim et al., Methylammonium chloride induces intermediate phase stabilization for efficient perovskite solar cells. Joule **3**(9), 2179–2192 (2019)
202. R.K. Singh et al., *Novel synthesis process of methyl ammonium bromide and effect of particle size on structural, optical and thermodynamic behavior of $CH_3NH_3PbBr_3$organometallic perovskite light harvester*. J. Alloys Compd. **743**, 728–736 (2018). https://doi.org/10.1016/j.jallcom.2018.01.355
203. Y. Wang et al., *A rutile TiO_2electron transport layer for the enhancement of charge collection for efficient perovskite solar cells*. Angew. Chem. Int. Ed. **58**(28), 9414–9418 (2019). https://doi.org/10.1002/anie.201902984
204. A. Bera et al., *Perovskite Oxide $SrTiO_3$as an Efficient Electron Transporter for Hybrid Perovskite Solar Cells*. J. Phys. Chem. C **118**(49), 28494–28501 (2014). https://doi.org/10.1021/jp509753p
205. D. Liu, T.L. Kelly, Perovskite solar cells with a planar heterojunction structure prepared using room-temperature solution processing techniques. Nat. Photonics **8**(2), 133–138 (2014). https://doi.org/10.1038/nphoton.2013.342
206. K. Mahmood et al., *Highly efficient perovskite solar cells based on a nanostructured WO_3–TiO_2* core–shell electron transporting material. J. Mater. Chem. A **3**(17), 9051–9057 (2015)
207. B. Yang et al., *Highly efficient semitransparent $CsPbIBr_2$ perovskite solar cells via low-temperature processed In_2S_3 as electron-transport-layer*. Nano Energy. **57**, 718–727 (2019)
208. Y.W. Noh et al., *Room-temperature synthesis of $ZrSnO_4$ nanoparticles for electron transport layer in efficient planar hetrojunction perovskite solar cells*. J. Mater. Sci. Technol. **42**, 38–45 (2020)
209. S.S. Shin et al., *Colloidally prepared La-doped $BaSnO_3$ electrodes for efficient, photostable perovskite solar cells*. Science. **356**(6334), 167–171 (2017). https://doi.org/10.1126/science.aam6620
210. P. Priya, A.A. Stonier, Emerging innovations in solar photovoltaic (PV) technologies: the perovskite solar cells and more. Energy Rep. **14**, 216–242 (2025). https://doi.org/10.1016/j.egyr.2025.06.003
211. W. Zhang et al., Strategies for improving efficiency and stability of inverted perovskite solar cells. Adv. Mater. **36**(37), 2311025 (2024). https://doi.org/10.1002/adma.202311025
212. J. Liu et al., Evolutionary manufacturing approaches for advancing flexible perovskite solar cells. Joule. **8**(4), 944–969 (2024). https://doi.org/10.1016/j.joule.2024.02.025
213. H. Wang et al., Recent progress in Large-Area perovskite photovoltaic modules. Trans. Tianjin Univ. **28**(5), 323–340 (2022). https://doi.org/10.1007/s12209-022-00341-y
214. F. Wang et al., Recent progress of scalable perovskite solar cells and modules. Energy Reviews. **1**(2), 100010 (2022). https://doi.org/10.1016/j.enrev.2022.100010
215. A. Agresti et al., Scalable deposition techniques for large-area perovskite photovoltaic technology: A multi-perspective review. Nano Energy. **122**, 109317 (2024). https://doi.org/10.1016/j.nanoen.2024.109317
216. Z. Hu, Z. Wang, P. Gao, Advancements in scaling up perovskite solar cells: from Small-Area devices to Large-Scale modules. ChemPhysChem. **25**(22), e202400587 (2024). https://doi.org/10.1002/cphc.202400587
217. F.U. Kosasih et al., Thermal evaporation and hybrid deposition of perovskite solar cells and mini-modules. Joule **6**(12), 2692–2734 (2022). https://doi.org/10.1016/j.joule.2022.11.004
218. E. Erdenebileg et al., Low-Temperature atomic layer deposited electron transport layers for Co-Evaporated perovskite solar cells. Solar RRL. **6**(1), 2100842 (2022). https://doi.org/10.1002/solr.202100842
219. T. Kim, J. Lim, S. Song, Recent progress and challenges of electron transport layers in Organic–Inorganic perovskite solar cells. Energies. **13** (2020). https://doi.org/10.3390/en13215572
220. A.O. Ali et al., Advancements in photovoltaic technology: A comprehensive review of recent advances and future prospects.

Energy Convers. Management: X. **26**, 100952 (2025). https://doi.org/10.1016/j.ecmx.2025.100952
221. N.J. Jeon et al., Solvent engineering for high-performance inorganic–organic hybrid perovskite solar cells. Nat. Mater. **13**(9), 897–903 (2014). https://doi.org/10.1038/nmat4014
222. M. Saliba et al., Incorporation of rubidium cations into perovskite solar cells improves photovoltaic performance. Science **354**(6309), 206–209 (2016). https://doi.org/10.1126/science.aah5557
223. G. Grancini, M.K. Nazeeruddin, Dimensional tailoring of hybrid perovskites for photovoltaics. Nat. Reviews Mater. **4**(1), 4–22 (2019). https://doi.org/10.1038/s41578-018-0065-0
224. M.H. Miah et al., Key degradation mechanisms of perovskite solar cells and strategies for enhanced stability: issues and prospects. RSC Adv. **15**(1), 628–654 (2025). https://doi.org/10.1039/d4ra07942f
225. A. Yadegarifard et al., FA/Cs-based mixed Pb–Sn perovskite solar cells: A review of recent advances in stability and efficiency. Nano Energy. **112**, 108481 (2023). https://doi.org/10.1016/j.nanoen.2023.108481
226. J. Ji et al., *Two-Stage Ultraviolet Degradation of Perovskite Solar Cells Induced by the Oxygen Vacancy-Ti^{4+} States*. iScience. **23**(4), 101013 (2020). https://doi.org/10.1016/j.isci.2020.101013
227. L. Lavagna et al., Platinum-free photoelectrochromic devices working with copper-based electrolytes for ultrastable smart windows. J. Mater. Chem. A **9**(35), 19687–19691 (2021). https://doi.org/10.1039/D1TA03544D
228. T. Chen, J. Xie, P. Gao, Ultraviolet photocatalytic degradation of perovskite solar cells: Progress, Challenges, and strategies. Adv. Energy Sustain. Res. **3**(6), 2100218 (2022). https://doi.org/10.1002/aesr.202100218
229. H.H. Park, *Modification of SnO_2 Electron transport layer in perovskite solar cells*. Nanomaterials. **12** (2022). https://doi.org/10.3390/nano12234326
230. A.U.I. Shah, E.L. Meyer, Perovskite-based solar cells in photovoltaics for commercial scalability: current progress, challenges, mitigations and future prospectus. Sol. Energy **286**, 113172 (2025). https://doi.org/10.1016/j.solener.2024.113172
231. M. Gantumur et al., Revolutionizing light capture: a comprehensive review of back-contact perovskite solar cell architectures. Mater. Today. (2025). https://doi.org/10.1016/j.mattod.2025.08.017
232. F.A. Vilela, R.R. Ciferri, 2021 *International Conference on Computational Science and Computational* Intelligence *(CSCI)*. 2021. https://doi.org/10.1109/CSCI54926.2021.00158
233. P. Mariani et al., Low-temperature strain-free encapsulation for perovskite solar cells and modules passing multifaceted accelerated ageing tests. Nat. Commun. **15**(1), 4552 (2024). https://doi.org/10.1038/s41467-024-48877-y
234. R. Ji et al., *Solvent-Free Fabrication Methods of Metal Halide Perovskites*. Advanced Materials, 2025. n/a(n/a): p. 2416604 https://doi.org/10.1002/adma.202416604
235. H.J. Kim, G.S. Han, H.S. Jung, *Managing the lifecycle of perovskite solar cells: Addressing stability and environmental concerns from utilization to end-of-life.* eScience, 2024. 4(2): p. 100243 https://doi.org/10.1016/j.esci.2024.100243
236. S. Apergi et al., Probing the reactivity of ZnO with perovskite precursors. ACS Appl. Mater. Interfaces. **16**(12), 14984–14994 (2024). https://doi.org/10.1021/acsami.4c01945
237. M.S. Hasan et al., Recent criterion on stability enhancement of perovskite solar cells. Processes. **10** (2022). https://doi.org/10.3390/pr10071408
238. T.D. Raju et al., Advancements in perovskites for solar cell commercialization: A review. Adv. Powder Mater. **4**(2), 100275 (2025). https://doi.org/10.1016/j.apmate.2025.100275
239. Q.A.K. Nisa, J.H. Kim, Emerging trends in interface processing: a comparative review of conventional and inverted perovskite solar cells. Adv. Industrial Eng. Chem. **1**(1), 13 (2025). https://doi.org/10.1007/s44405-025-00013-0
240. Z. Wang et al., Recent advances in interfacial engineering for high-efficiency perovskite photovoltaics. DeCarbon. **8**, 100107 (2025). https://doi.org/10.1016/j.decarb.2025.100107